NASA
TP
2005
c.1

NASA
Technical
Paper
2005

April 1982

TECH LIBRARY KAFB, NM
0067778

# Effects of Axisymmetric and Normal Air Jet Plumes and Solid Plume on Cylindrical Afterbody Pressure Distributions at Mach Numbers From 1.65 to 2.50

Peter F. Covell

LOAN COPY RETURN TO
AFWL TECHNICAL LIBRARY
KIRTLAND AFB, N. M.

29 APR 1982
Technical Library
AFWL (DOUL)
Kirtland AFB, NM 87117

NASA

TECH LIBRARY KAFB, NM
0067778

NASA
Technical
Paper
2005

1982

# Effects of Axisymmetric and Normal Air Jet Plumes and Solid Plume on Cylindrical Afterbody Pressure Distributions at Mach Numbers From 1.65 to 2.50

Peter F. Covell
*Langley Research Center*
*Hampton, Virginia*

NASA
National Aeronautics
and Space Administration

**Scientific and Technical
Information Branch**

## SUMMARY

An experimental wind-tunnel investigation has been conducted to determine simulated rocket plume interference effects due to various plume simulation devices. Afterbody pressure distributions and base pressures were measured on a strut-mounted ogive-cylinder afterbody model. A series of axisymmetric air nozzles, a solid plume, and a normal air jet nozzle were tested on the model at Mach numbers from 1.65 to 2.50, a Reynolds number per meter of $6.56 \times 10^6$, and an angle of attack of 0°. The axisymmetric nozzles, which varied in exit lip Mach number from 1.7 to 2.7, were designed to produce a selected underexpanded plume shape for conditions of no external flow. The solid plume matched this plume shape. The normal air jet nozzle consisted of two circumferential rows of orifices which discharged perpendicular to the longitudinal axis and downstream of the model base.

The solid plume induces greater afterbody disturbances and base pressures than those induced by the axisymmetric nozzle plumes at the selected underexpanded conditions, and the differences increase with Mach number. The plume-induced afterbody disturbance distance and base pressure for each axisymmetric air nozzle can be correlated with the induced effects of the other air nozzles by matching a thrust coefficient parameter which is based on nozzle lip conditions. At constant base pressures, the normal air jet plume and solid plume induce afterbody disturbance distances that agree to within about 1/10 body diameter with those induced by the axisymmetric plumes, except at plateau base pressures associated with high thrust levels.

## INTRODUCTION

The interaction of a rocket exhaust plume with the flow over a missile can affect performance, stability, and control characteristics. This interaction arises because the exhaust plume produced by a rocket nozzle operating at underexpanded conditions interferes with the external flow such that the afterbody flow field and base pressures are affected. Previous investigations have been conducted by using air and gas-powered axisymmetric nozzle plumes, normal air jets which exhaust perpendicular to the body longitudinal axis, and solid plumes to simulate an axisymmetric rocket exhaust plume (refs. 1 to 7). The solid plume and normal air jet plume simulators are usually employed on sting-mounted force models where the axisymmetric nozzle is not practical. Efforts to correlate the interference effects of these simulation methods with each other or with flight or rocket sled data (refs. 8 and 9), particularly at supersonic speeds, have been limited (ref. 10). Reference 11 contains comparisons made between several plume simulation devices at transonic speeds.

The purpose of this investigation was to measure and correlate the afterbody interference effects induced by various axisymmetric air jet plumes, normal air jet plumes, and a solid plume at supersonic free-stream Mach numbers. Four axisymmetric nozzles with different exit lip Mach numbers and exit angles were designed according to the method of reference 12 to produce congruent exhaust plume geometries over the initial expansion region at one selected underexpanded nozzle operating condition. The effects of the external flow on the air plume boundary were not considered in the analysis. A solid plume simulator with the same geometry as the selected under-

expanded design air plume was tested for comparison with the air plumes. The axisymmetric air nozzles were operated over a range of jet pressure ratios so that nozzle operating parameters could be determined which correlate the plume-induced effects for the different nozzles. The normal jet plume simulator nozzle was designed to produce a variable disk-shaped air plume downstream of the model base. The normal jet plume-induced effects were compared and correlated with those induced by the axisymmetric plumes.

In this investigation, the afterbody pressure distributions and base pressures were measured on a strut-mounted ogive-cylinder body. Tests were run at free-stream Mach numbers of 1.65, 2.00, and 2.50 with angles of attack and sideslip maintained at 0°.

## SYMBOLS

| | |
|---|---|
| A | area, $cm^2$ |
| $C_p$ | pressure coefficient, $\frac{p - p_\infty}{q_\infty}$ |
| $C_T$ | thrust coefficient, $\frac{\text{Thrust}}{q_\infty A_b}$ |
| D | body diameter, cm |
| M | Mach number |
| M.S. | model station |
| p | static pressure, Pa |
| $p_{t,j}$ | jet total pressure, Pa |
| q | dynamic pressure, Pa |
| r | radial distance from model center line, cm |
| x | distance measured upstream from base, cm |
| $\gamma$ | ratio of specific heats, 1.4 for air |
| $\sigma$ | disturbance distance, cm |

Subscripts:

| | |
|---|---|
| b | base |
| e | exit |
| $\ell$ | lip |
| nj | normal jet |
| r | radial |

t throat

∞ free-stream conditions

## MODEL AND APPARATUS

The test model consisted of an ogive-cylinder body mounted on a strut which supplied high pressure air to the model plenum. (See fig. 1.) Interchangeable afterbody-nozzle sections contained 10 surface static-pressure orifices and a base pressure manifold located opposite the strut. (See fig. 2.) A photograph of the model installed in the wind tunnel is shown as figure 3. The strut was inclined 60° from the vertical in order to locate the model near the center of the test section.

The four axisymmetric air nozzles were designed to produce a selected geometrically congruent exhaust plume shape over the initial expansion region. The analysis used in the design is the method proposed in reference 12 which uses an improved method of characteristics to determine the initial expansion angle and radius of curvature of the plume. This circular arc approximation is shown in reference 12 to match the plume geometry as predicted by the method of characteristics solution over about 1 nozzle exit radius from the base plane. The effects of the free-stream flow are not considered. Nozzle design is accomplished by selecting an exit lip Mach number and external ambient pressure and varying the nozzle lip angle and exit pressure to achieve the design plume geometry. With the lip angle established, the nozzle throat is designed to produce the selected exit lip Mach number. For the wind-tunnel tests, the ratio of jet total pressure to base pressure was selected as the nozzle operating parameter rather than the conventional jet pressure ratio since the plume expansion is initially influenced by the local base conditions. Figure 4 shows the nozzle geometries, and their coordinates are given in table I.

The solid plume simulator, which matches the selected underexpanded air plume geometry, is shown in figure 5. Also shown is the normal jet nozzle, which consists of 2 circumferential rows of 12 orifices each, located 0.66 body diameter downstream of the base, and discharges normal to the longitudinal axis of the model.

## DATA REDUCTION

The thrust coefficient for the axisymmetric air nozzles is computed by using the following one-dimensional isentropic equation:

$$C_T = \frac{A_e}{q_\infty A_b}\left[\gamma p_e M_e^2 + (p_e - p_\infty)\right]$$

$$= \frac{A_e}{q_\infty A_b}\left[p_{t,j}\left(\frac{p_e}{p_{t,j}}\right)\left(\gamma M_e^2 + 1\right) - p_\infty\right]$$

The conditions at the exit, $M_e$ and $p_e$, were determined from the nozzle area ratio and one-dimensional isentropic relationships.

The correlation parameter $C_{T,\ell}$ (thrust coefficient based on lip conditions) is computed by using the following thrust coefficient equation.

$$C_{T,\ell} = \frac{A_e}{q_\infty A_b}\left[p_{t,j}\left(\frac{p_\ell}{p_{t,j}}\right)\left(\gamma M_\ell^2 + 1\right) - p_\infty\right]$$

Note that the exit Mach number is replaced by the lip Mach number and the exit pressure is replaced by the lip pressure. The lip Mach number is obtained from the analysis in reference 12 and is utilized in the one-dimensional isentropic relationship for determining the lip pressure.

The radial thrust for the normal jet plume simulator is defined as the sum of the magnitudes of the thrusts of each radially exhausting orifice, and the radial thrust coefficient is computed as follows:

$$C_{T,r} = \frac{24A_{e,nj}}{q_\infty A_b}\left[p_{t,j}\left(\frac{p_e}{p_{t,j}}\right)\left(\gamma M_e^2 + 1\right) - p_\infty\right]$$

where $\frac{p_e}{p_{t,j}} = 0.5283$.

## TEST CONDITIONS

The tests were conducted in the Langley Unitary Plan Wind Tunnel at Mach numbers of 1.65, 2.00, and 2.50; a Reynolds number per meter of $6.56 \times 10^6$; and stagnation temperature of 325 K. A detailed description and calibration of this facility is presented in reference 13. The tunnel dew point and model air jet dew point were maintained sufficiently low to insure negligible condensation effects in the test section and model nozzles. Tests were conducted for jet pressure ratios up to 615 which produced ratios of jet total pressure to base pressure of up to 275. Model plenum stagnation temperature varied between 300 K and 311 K. Model angle of attack and angle of sideslip were maintained at 0°.

## RESULTS AND DISCUSSION

A comparison of the afterbody pressure distributions for the four axisymmetric air nozzles at the selected underexpanded plume design conditions and for the solid plume is shown in figure 6. Table II contains a listing of the nozzle operating parameters for these plume design conditions. The solid plume induces higher afterbody pressures which also extend further upstream than do those induced by the design air plumes. The difference in the maximum afterbody pressure increases as the free-stream Mach number increases. Base pressures for these same conditions are shown in figure 7, and as the free-stream Mach number increases, the solid plume induces base pressures much higher than do the air plumes. The differences between the solid and

air plume results as indicated in figures 6 and 7 show that the external free-stream flow significantly alters the effective geometry of the air plumes outside the base region.

The afterbody pressure distributions for the four axisymmetric air nozzles operating over a range of underexpanded conditions are presented in figure 8. The afterbody pressures increase and the disturbed flow region moves upstream of the base as the thrust coefficient increases. The plateau afterbody pressures increase with free-stream Mach number.

Schlieren photographs (fig. 9) indicate a separated flow region on the afterbody associated with the disturbed flow region noted in the pressure distributions. Although the actual occurrence of boundary-layer separation was not determined during this test, previous investigations have noted that separation occurs slightly downstream of the pressure rise (ref. 14). Analysis of jet-off afterbody pressure distributions show that the shocks which appear to cross the afterbody at $M_\infty = 1.65$ produce negligible interference effects.

In order to quantitatively define the afterbody disturbance effects, a disturbance distance $\sigma$ was defined as the distance from the base of the model to the point where the plume-induced pressure rise intersects the jet-off pressure distribution. The results in figure 10 indicate a nearly linear variation of the disturbance distance with the nozzle thrust coefficient for the four axisymmetric air nozzles. Note that the typical disturbance distance uncertainty due to pressure distribution curve fairing corresponds to the distance between the static-pressure orifices on the afterbody. The variation of base pressure coefficient with thrust coefficient is shown in figure 11. The base pressures correlate as a function of thrust coefficient. The parameter $C_{T,\ell}$, which resembles the nozzle thrust coefficient but is computed with nozzle lip conditions, was found to reduce the data scatter, particularly for the disturbance distance results. (See figs. 12 and 13.) With $C_{T,\ell}$ as the correlation parameter, figure 14 summarizes the interference characteristics induced by all four air nozzles. At constant $C_{T,\ell}$, the disturbance distance and the base pressure coefficient decreases as free-stream Mach number increases.

Presented in figure 15 are the afterbody pressure distributions for the normal air jet model. As the radial thrust coefficient increases, the afterbody pressures increase to a plateau value, and the pressure increases extend further upstream. The results in figure 16 show that the variation of the disturbance distance with the radial thrust coefficient is nearly linear and insensitive to free-stream Mach number change. For values of $\sigma/D$ greater than 0.2, the uncertainty band increases because of the greater pressure orifice spacing. The variation of base pressure coefficient with radial thrust coefficient (fig. 17) does change with free-stream Mach number at a constant radial thrust coefficient. Schlieren photographs of the normal air jet plume are shown in figure 18.

A comparison of the interference effects induced by the normal air jet and the axisymmetric air plumes is shown in figure 19. By matching the base pressure, the afterbody disturbance distance induced by the normal jet matches that of the axisymmetric plume within approximately 1/10 body diameter for conditions well below the plateau base pressures. The base pressure has been shown to correlate afterbody disturbance effects between axisymmetric and normal jet plumes at transonic speeds (ref. 11). At the plateau base pressures, which correspond to high thrust levels, the disturbance distance varies greatly, and the differences between the normal and axisymmetric jet plume effects are much larger. Also shown in figure 19 are the

results for the solid plume which, with the base pressure as the correlation parameter, induces disturbance distances that nearly match those induced by the axisymmetric air plumes. In order to utilize the solid plume or the normal jet to simulate plume disturbances, it is necessary to have data on the induced base pressures for the axisymmetric nozzle that is being simulated.

## CONCLUSIONS

A wind-tunnel investigation has been conducted to determine the simulated rocket plume interference effects on a strut-mounted ogive-cylinder afterbody model. Axisymmetric air nozzles, a solid plume, and a normal jet nozzle were tested at Mach numbers of 1.65, 2.00, and 2.50 with a Reynolds number per meter of $6.56 \times 10^6$. Angles of attack and sideslip were held constant at 0°.

The axisymmetric air nozzles were designed to produce congruent plume shapes for the condition of no external flow. Exit lip Mach numbers of the four test nozzles were 1.7, 2.0, 2.4, and 2.7. The solid plume geometry matches the underexpanded design plume shape produced by the axisymmetric nozzles. The normal jet nozzle consisted of 2 circumferential rows of 12 orifices each and discharged perpendicular to the longitudinal axis and downstream of the base of the body.

The results of this study indicate the following conclusions:

1. The solid plume induces afterbody pressure disturbances which extend further upstream and higher base pressures than those induced by the axisymmetric nozzle plumes at the selected underexpanded design condition. These differences increase with free-stream Mach number.

2. The plume-induced disturbance distance and base pressure for each axisymmetric air nozzle can be correlated with the induced effects of the other axisymmetric nozzles by matching the thrust coefficient based on nozzle lip conditions.

3. At the same base pressure, the normal air jet and solid plume induce afterbody disturbance distances that match to within about 1/10 body diameter with those induced by the axisymmetric jet plumes except at plateau base pressures associated with very high thrust levels.

Langley Research Center
National Aeronautics and Space Administration
Hampton, VA 23665
March 11, 1982

REFERENCES


1. Rubin, Donald V.; Brazzel, Charles E.; Henderson, James H.: The Effects of Jet Plume and Boattail Geometry on Base and Afterbody Pressures of a Body of Revolution at Mach Numbers of 2.0 to 3.5. Rep. No. RD-TR-70-5, U.S. Army, Apr. 6, 1970. (Available from DTIC as AD 871 651.)

2. Craft, Joseph C.; and Brazzel, Charles E.: An Experimental Investigation of Base Pressure on a Body of Revolution at High Thrust Levels and Free Stream Mach Numbers of 1.5 to 2.87. Rep. No. RD-TM-70-6, U.S. Army, July 31, 1970. (Available from DTIC as AD 875 042.)

3. Burt, James R., Jr.; Henderson, James H.; Pettis, Wiley, Jr.: The Effects of Three Rocket Jet Plume Simulators on the Aerodynamic Characteristics of Several Missile Configurations. Rep. No. RD-TR-70-20, U.S. Army, Sept. 10, 1970. (Available from DTIC as AD 877 497.)

4. Dods, Jules B., Jr.; Brownson, Jack J.; Kassner, Donald L.; Blackwell, Kenneth L.; Decker, John P.; and Roberts, Barney B.: Effect of Gaseous and Solid Simulated Jet Plumes on a 040A Space Shuttle Launch Configuration at M = 1.6 to 2.2. NASA TM X-3032, 1974.

5. Batiuk, George; and Henderson, James H.: A Summary of Jet Plume Effects on the Stability Characteristics of a Body of Revolution With Various Fin Configurations at Mach Numbers From 0.2 to 2.3 (Normal Jet Plume Simulator). Tech. Rep. RD-77-12, U.S. Army, Dec. 13, 1976. (Available from DTIC as AD A037 356.)

6. Henderson, James H.: Investigation of Jet Plume Effects on the Longitudinal Stability Characteristics of a Body of Revolution With Various Fin Configurations at Mach Numbers From 0.2 to 2.3 (Normal Jet Plume Simulator). Tech. Rep. RD-76-22, U.S. Army, Feb. 20, 1976. (Available from DTIC as AD A024 978.)

7. Blackwell, Kenneth L.; and Hair, Leroy M.: Space Shuttle Afterbody Aerodynamics/ Plume Simulation Data Summary. NASA TP-1384, 1978.

8. Alpinieri, L. J.; and Adams, Richard H.: Flow Separation Due to Jet Pluming. AIAA J., vol. 4, no. 10, Oct. 1966, pp. 1865-1866.

9. Martin, T. A.; and Deep, Raymond A.: Some Applications of a Test Track for Aerodynamic Testing. AIAA Paper 78-167, Jan. 1978.

10. Korst, H. H.; White, R. A.; Nyberg, S.-E.; and Agrell, J.: The Simulation and Modeling of Jet Plumes in Wind Tunnel Facilities. A Collection of Technical Papers - AIAA 11th Aerodynamic Testing Conference, Mar. 1980, pp. 104-116. (Available as AIAA-80-0430.)

11. Burt, James Robert, Jr.: An Investigation of the Effectiveness of Several Devices in Simulating a Rocket Plume at Free Stream Mach Numbers of 0.9 to 1.2. Rep. No. RD-TR-71-22, U.S. Army, Sept. 30, 1971. (Available from DTIC as AD 734 323.)

12. Korst, H. H.: Approximate Determination of Jet Contours Near the Exit of Axially Symmetrical Nozzles as a Basis for Plume Modeling. RD-TR-72-14, U.S. Army, Aug. 1972. (Available from DTIC as AD 756 380.)

13. Jackson, Charlie M., Jr.; Corlett, William A.; and Monta, William J.: Description and Calibration of the Langley Unitary Plan Wind Tunnel. NASA TP-1905, 1981.

14. Price, Earl A., Jr.; and Stallings, Robert L., Jr.: Investigation of Turbulent Separated Flows in the Vicinity of Fin-Type Protuberances at Supersonic Mach Numbers. NASA TN D-3804, 1967.

TABLE I.- NOZZLE GEOMETRY

| $M_\ell$ = 1.7 | | $M_\ell$ = 2.0 | | $M_\ell$ = 2.4 | | $M_\ell$ = 2.7 | |
|---|---|---|---|---|---|---|---|
| x | r | x | r | x | r | x | r |
| -2.428 | [a]2.438 | | | -3.475 | [a]2.438 | | |
| -1.242 | [b]2.282 | -2.555 | [a]2.438 | -1.248 | [b]1.842 | | |
| -1.146 | 2.271 | -1.256 | [b]2.090 | -1.152 | 1.821 | | |
| -1.051 | 2.260 | -1.152 | 2.072 | -1.061 | 1.802 | | |
| -0.957 | 2.250 | -1.050 | 2.056 | -0.971 | 1.784 | | |
| -0.864 | 2.242 | -0.949 | 2.042 | -0.883 | 1.769 | -4.052 | [a]2.438 |
| -0.771 | 2.234 | -0.849 | 2.029 | -0.795 | 1.754 | -1.323 | [b]1.707 |
| -0.677 | 2.227 | -0.748 | 2.017 | -0.707 | 1.742 | -1.108 | 1.660 |
| -0.584 | 2.221 | -0.647 | 2.007 | -0.618 | 1.730 | -0.913 | 1.625 |
| -0.488 | 2.215 | -0.543 | 1.998 | -0.531 | 1.720 | -0.728 | 1.596 |
| -0.326 | 2.209 | -0.362 | 1.986 | -0.438 | 1.711 | -0.548 | 1.575 |
| -0.163 | 2.204 | -0.181 | 1.978 | -0.219 | 1.697 | -0.359 | 1.558 |
| 0 | [c]2.203 | 0 | [c]1.976 | 0 | [c]1.692 | 0 | [c]1.546 |
| 0.163 | 2.204 | 0.181 | 1.978 | 0.219 | 1.697 | 0.359 | 1.558 |
| 0.326 | 2.209 | 0.362 | 1.986 | 0.483 | 1.711 | 0.548 | 1.575 |
| 0.488 | 2.215 | 0.543 | 1.998 | 0.531 | 1.720 | 0.728 | 1.596 |
| 0.584 | 2.221 | 0.647 | 2.007 | 0.618 | 1.730 | 0.913 | 1.625 |
| 0.677 | 2.227 | 0.748 | 2.017 | 0.707 | 1.742 | 1.108 | 1.660 |
| 0.771 | 2.234 | 0.849 | 2.029 | 0.795 | 1.754 | 1.323 | 1.707 |
| 0.864 | 2.242 | 0.949 | 2.042 | 0.883 | 1.769 | 1.575 | 1.770 |
| 0.957 | 2.250 | 1.050 | 2.056 | 0.971 | 1.784 | 1.891 | 1.861 |
| 1.051 | 2.260 | 1.152 | 2.072 | 1.061 | 1.802 | 2.316 | 1.999 |
| 1.146 | 2.271 | 1.256 | 2.090 | 1.152 | 1.821 | 2.929 | 2.228 |
| 1.242 | 2.282 | 1.426 | 2.122 | 1.248 | 1.842 | 3.591 | [d]2.501 |
| 1.340 | 2.295 | 1.675 | 2.175 | 1.344 | 1.865 | 3.681 | [e]2.540 |
| 1.441 | 2.309 | 1.810 | [d]2.207 | 1.447 | 1.891 | | |
| 1.545 | 2.325 | 3.188 | [e]2.540 | 1.555 | 1.920 | | |
| 1.628 | [d]2.337 | | | 1.671 | 1.952 | | |
| 2.893 | [e]2.540 | | | 1.796 | 1.990 | | |
| | | | | 1.932 | 2.033 | | |
| | | | | 2.081 | 2.083 | | |
| | | | | 2.189 | [d]2.120 | | |
| | | | | 3.386 | [e]2.540 | | |

[a]Nozzle entrance.
[b]Upstream tangent point.
[c]Throat.
[d]Downstream tangent point.
[e]Nozzle exit.

TABLE II.- NOZZLE DESIGN AND TEST CONDITIONS

| Design conditions | | | Test conditions | | | | | | | | | | | |
|---|---|---|---|---|---|---|---|---|---|---|---|---|---|---|
| | | | $M_\infty = 1.65$ | | | | $M_\infty = 2.00$ | | | | $M_\infty = 2.50$ | | | |
| $M_\ell$ | $M_e$ | $p_{t,j}/p_b$ | $p_{t,j}/p_b$ | $p_{t,j}/p_\infty$ | $C_T$ | $C_{T,\ell}$ | $p_{t,j}/p_b$ | $p_{t,j}/p_\infty$ | $C_T$ | $C_{T,\ell}$ | $p_{t,j}/p_b$ | $p_{t,j}/p_\infty$ | $C_T$ | $C_{T,\ell}$ |
| 1.70 | 1.69 | 39.6 | 40.6 | 63.4 | 21.6 | 21.4 | 39.8 | 53.4 | 12.3 | 12.2 | 39.3 | 37.4 | 5.5 | 5.4 |
| 2.00 | 1.97 | 55.1 | 56.0 | 91.0 | 26.0 | 25.4 | 55.0 | 84.2 | 16.4 | 16.0 | 54.6 | 61.7 | 7.6 | 7.5 |
| 2.40 | 2.33 | 82.4 | 82.4 | 137.2 | 29.9 | 28.2 | 82.3 | 135.1 | 20.0 | 18.9 | | | | |
| 2.70 | 2.53 | 108.2 | 109.0 | 181.4 | 33.6 | 29.0 | 108.1 | 177.4 | 22.3 | 19.3 | 108.9 | 145.4 | 11.7 | 10.1 |

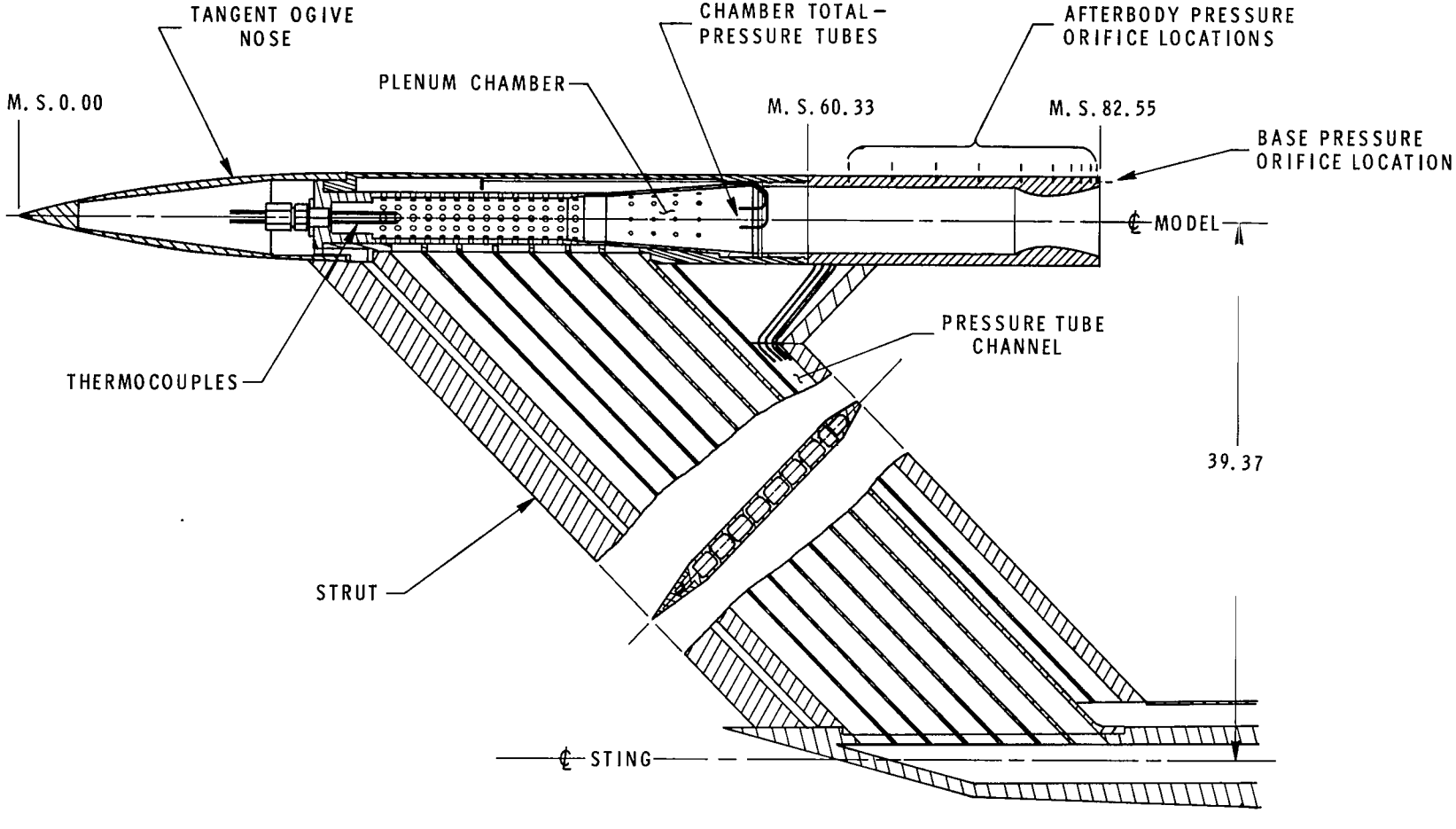


Figure 1.- Sketch of model and strut detail. All dimensions are in centimeters.

ORIFICE DISTANCE FROM BASE

| 1 | 2 | 3 | 4 | 5 | 6 | 7 | 8 | 9 | 10 |
|---|---|---|---|---|---|---|---|---|---|
| 18.57 | 15.40 | 12.22 | 9.05 | 5.87 | 3.49 | 2.06 | 1.43 | 0.79 | 0.16 |

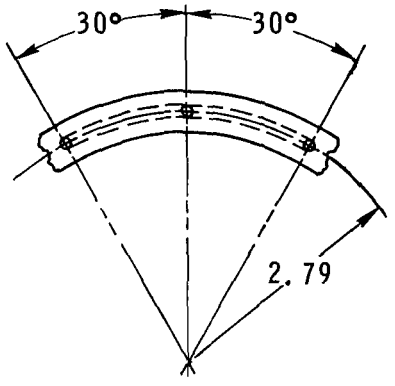


BASE PRESSURE MANIFOLD

SECTION A-A

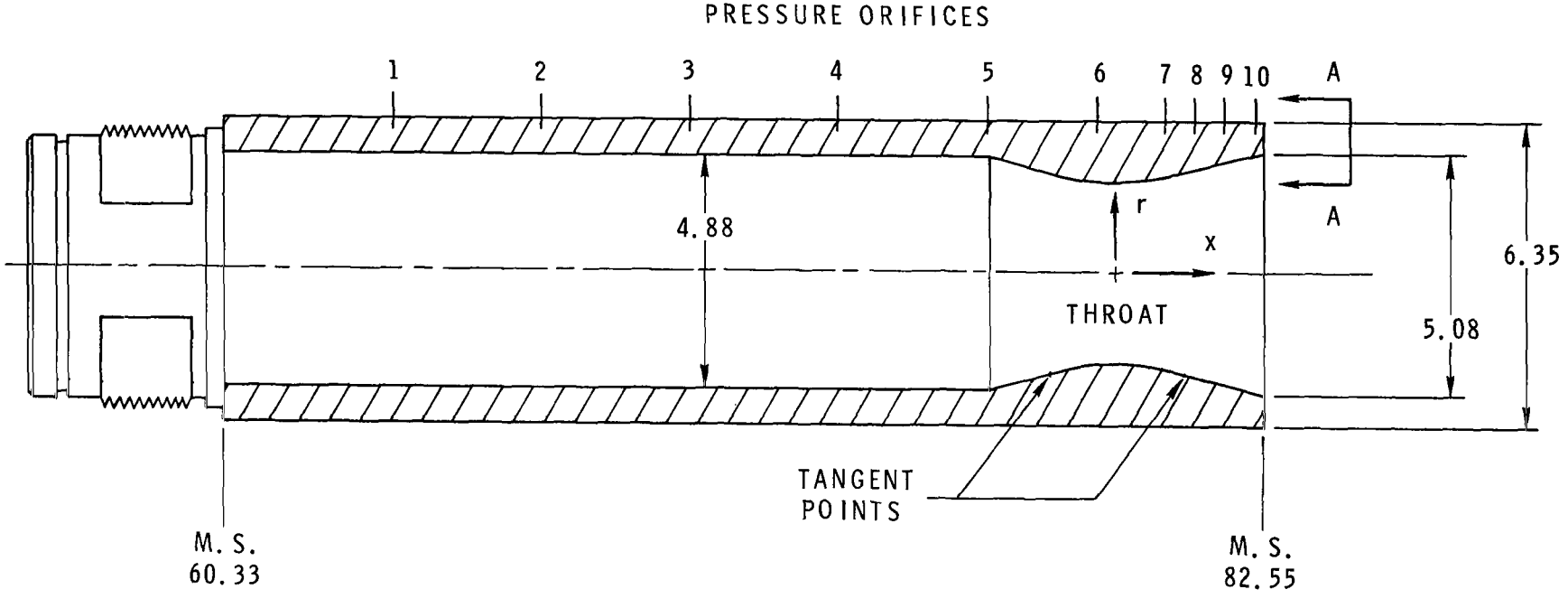


Figure 2.- Afterbody-nozzle detail. All dimensions are in centimeters.

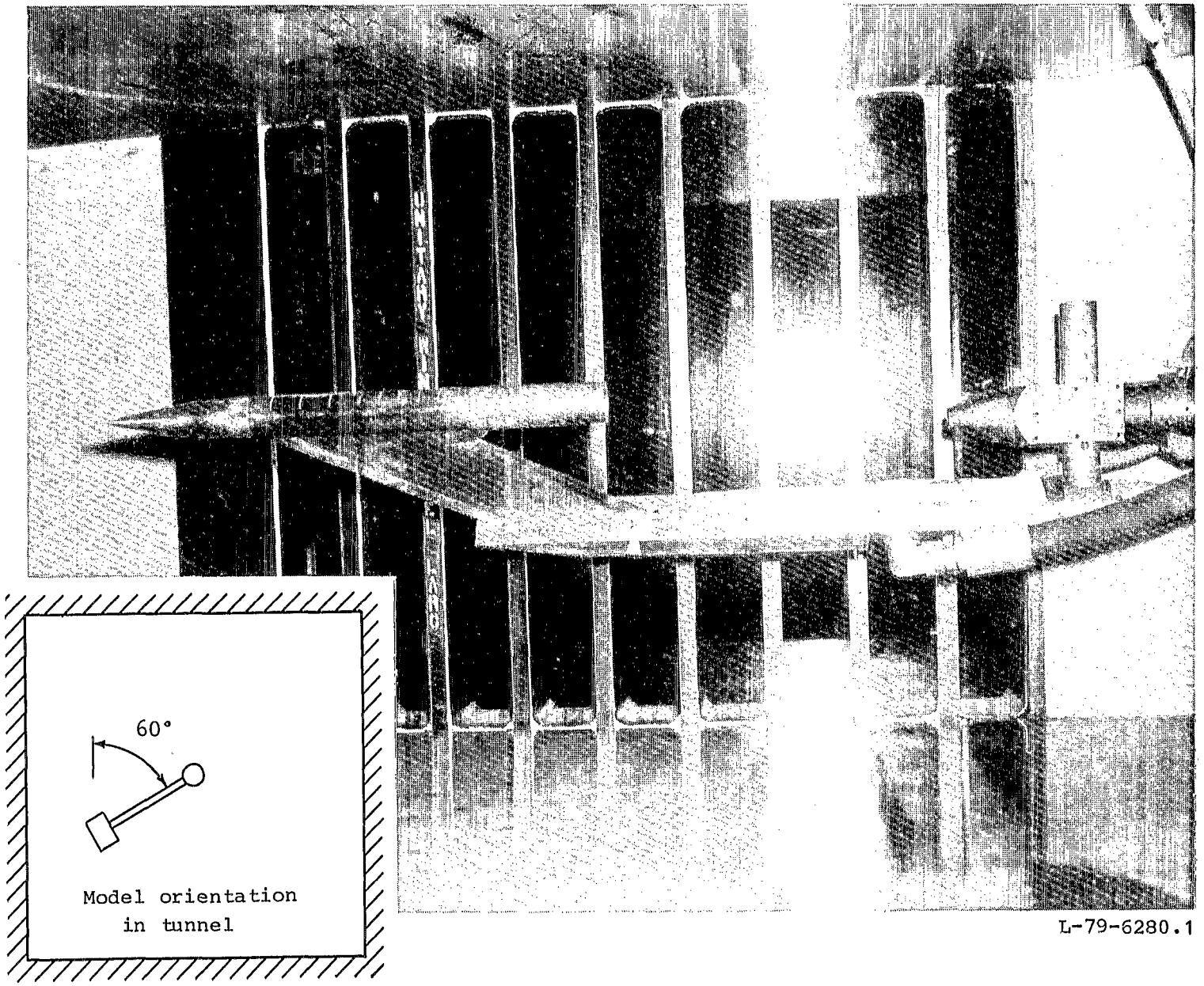


L-79-6280.1

Figure 3.- Model in wind tunnel.

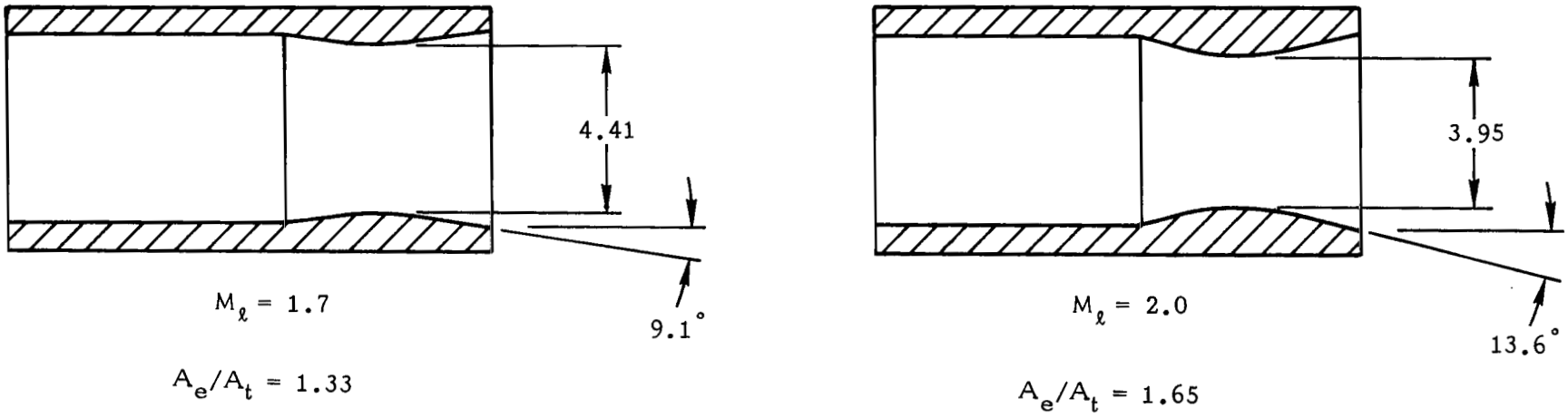


EXIT DIAMETER = 5.08

FOR ALL NOZZLES

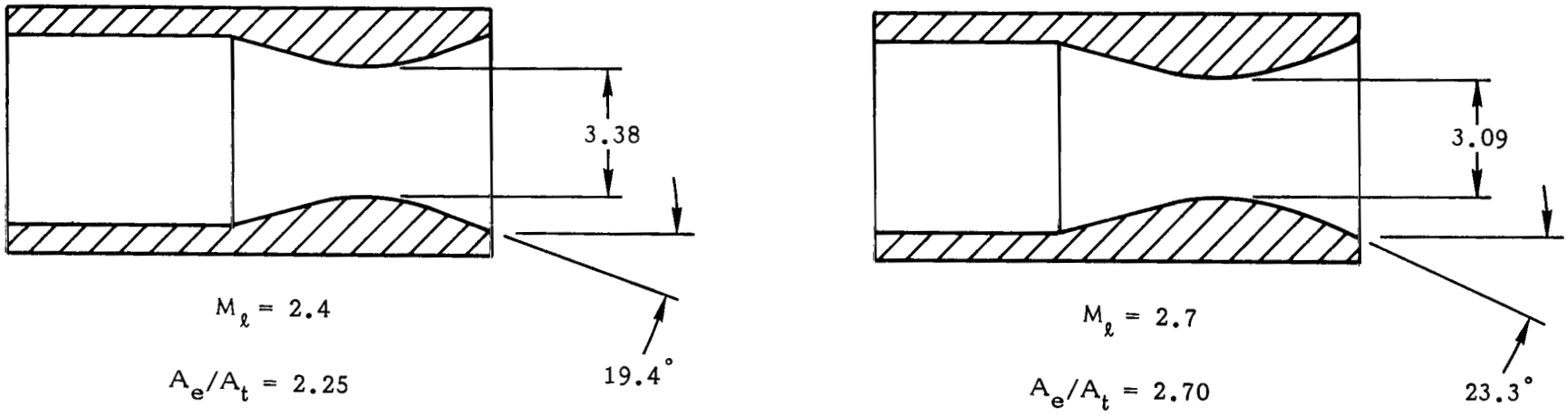


Figure 4.- Nozzle detail. All dimensions are in centimeters.

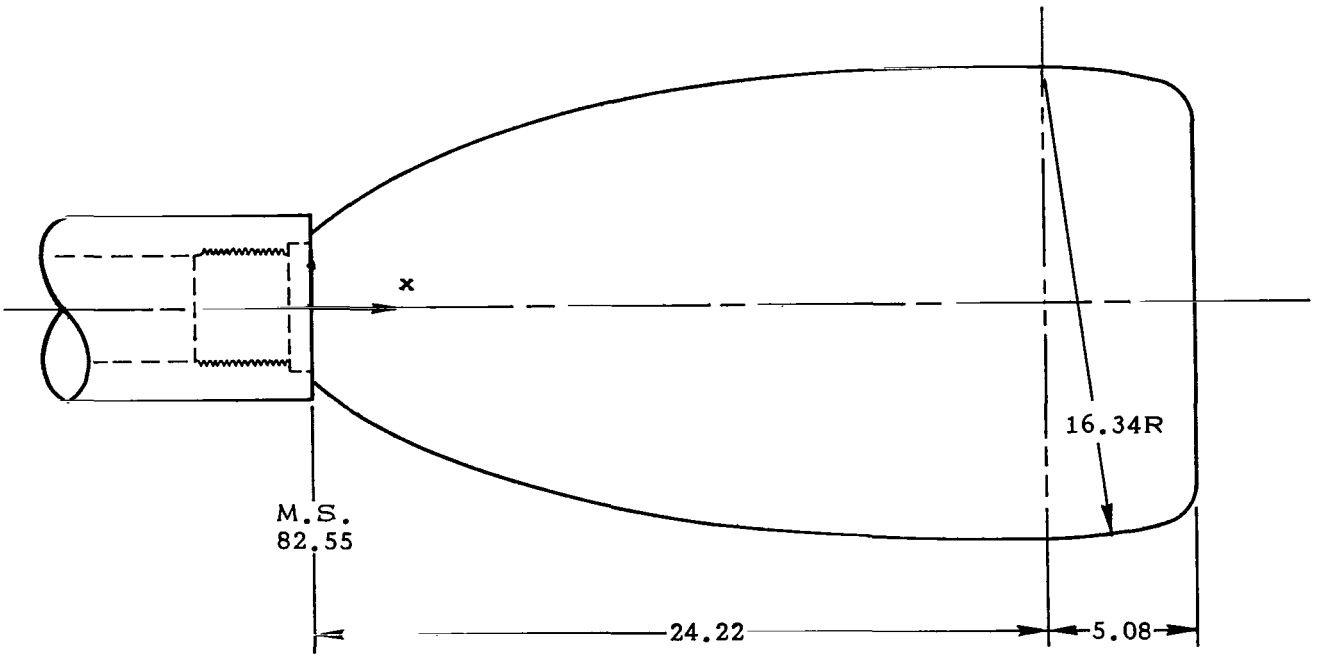


SOLID PLUME
COORDINATES

| x | r |
|---|---|
| 0.00 | 2.54 |
| 0.60 | 3.05 |
| 0.92 | 3.30 |
| 1.27 | 3.56 |
| 2.05 | 4.06 |
| 2.95 | 4.57 |
| 3.98 | 5.08 |
| 4.55 | 5.33 |
| 5.85 | 5.84 |
| 6.57 | 6.10 |
| 7.37 | 6.35 |
| 8.25 | 6.60 |
| 9.25 | 6.86 |
| 10.37 | 7.11 |
| 11.65 | 7.37 |
| 13.18 | 7.62 |
| 15.22 | 7.87 |
| 18.54 | 8.10 |
| 24.22 | 8.17 |

NORMAL JET NOZZLE

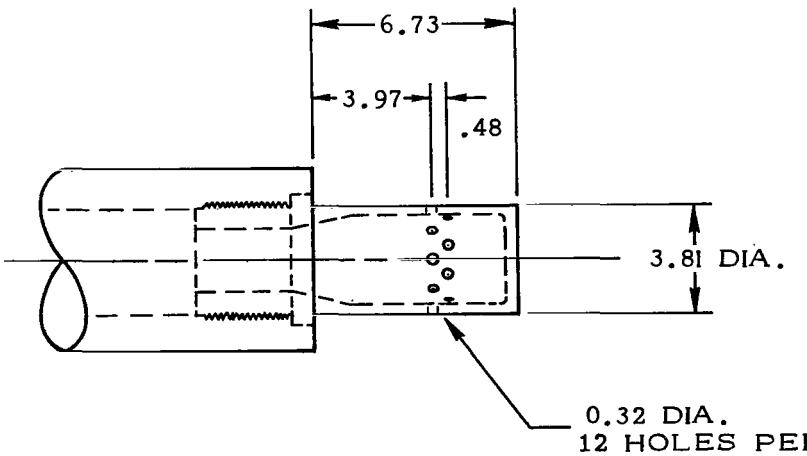


Figure 5.- Solid plume and normal jet nozzle geometries.
All dimensions are in centimeters.

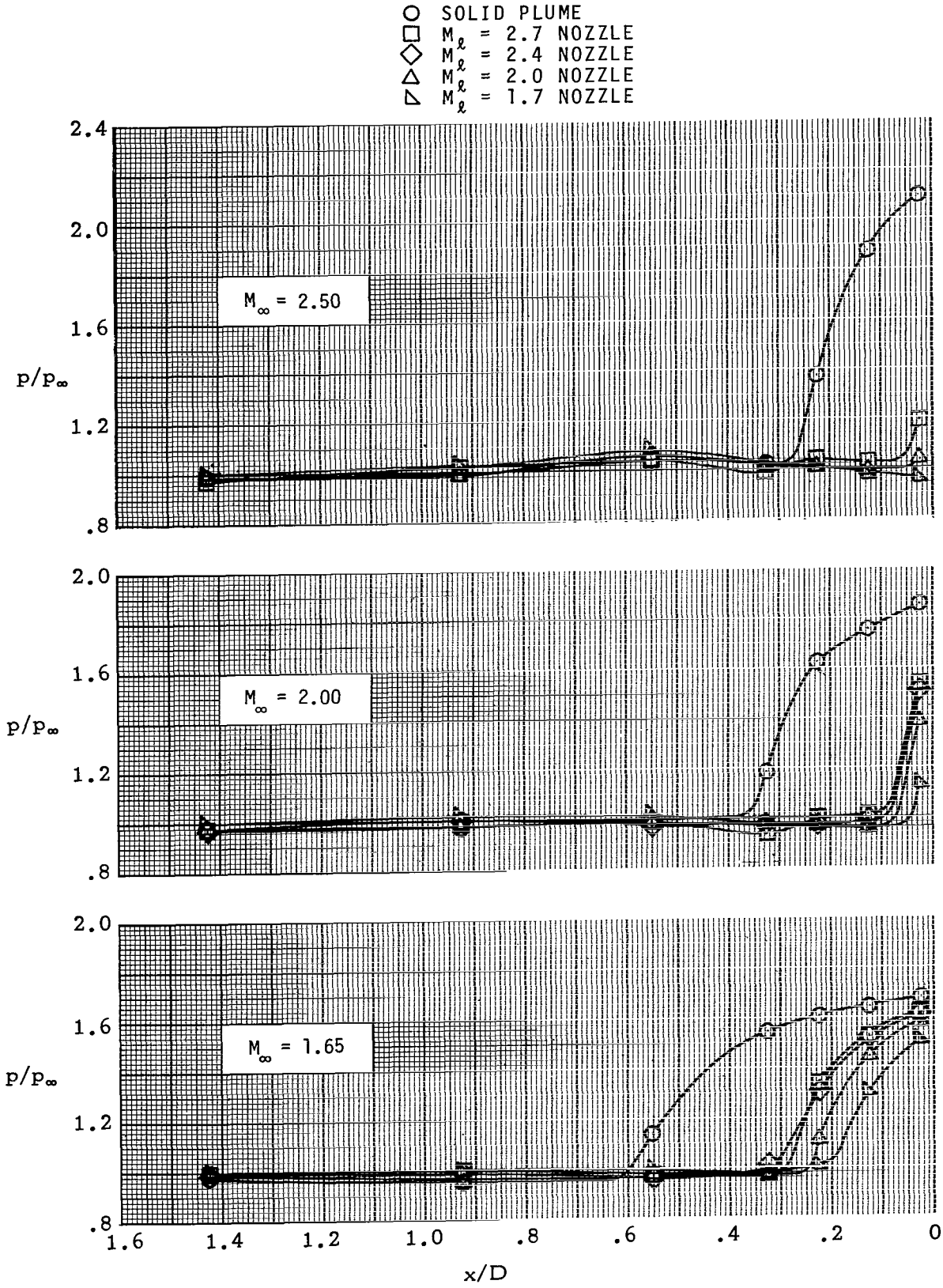


Figure 6.- Afterbody pressure distributions for axisymmetric nozzles at design $p_{t,j}/p_b$ and for solid plume.

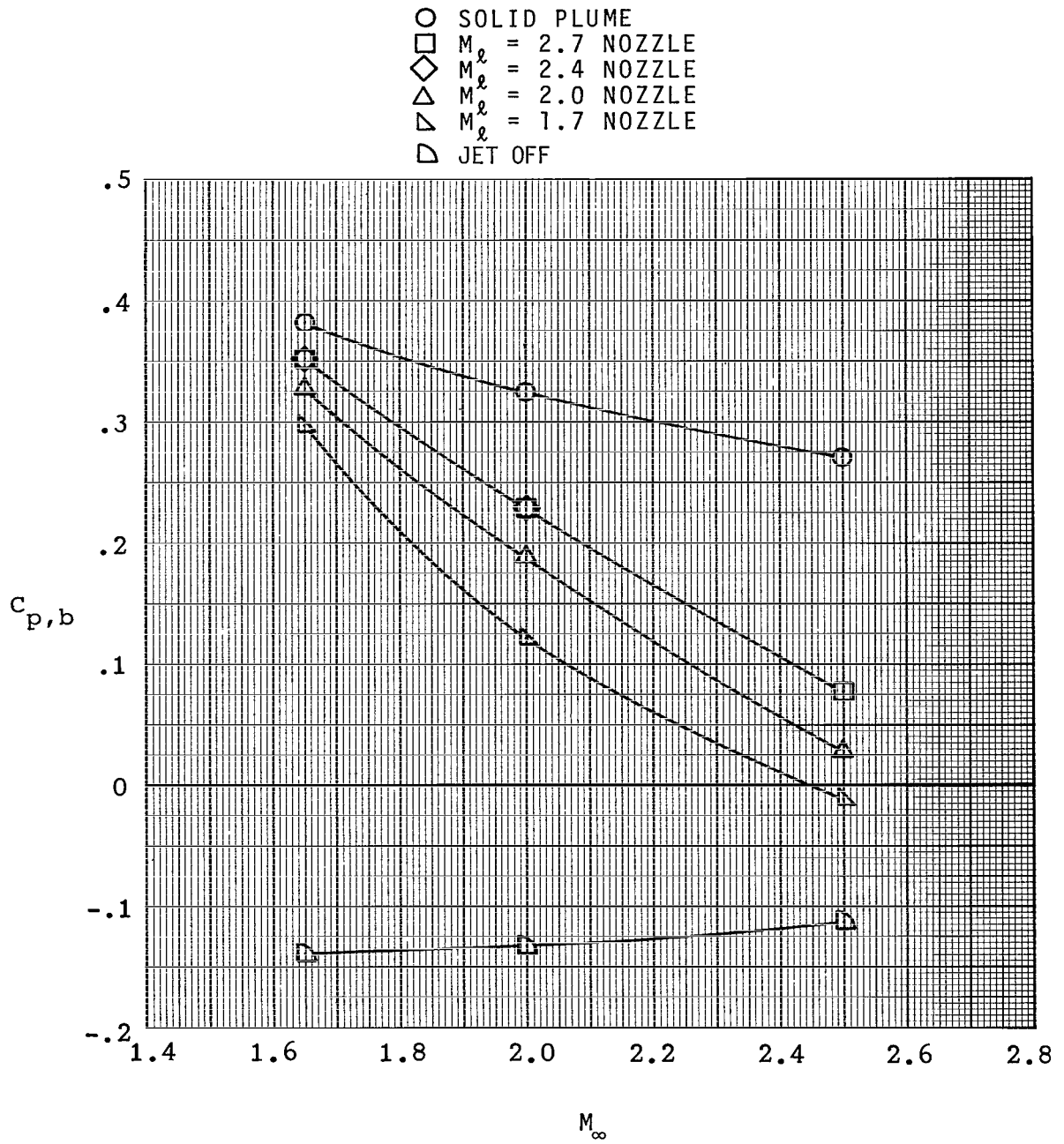


Figure 7.- Variation of base pressure coefficient with free-stream Mach number for axisymmetric nozzles at design $p_{t,j}/p_b$ and for solid plume.

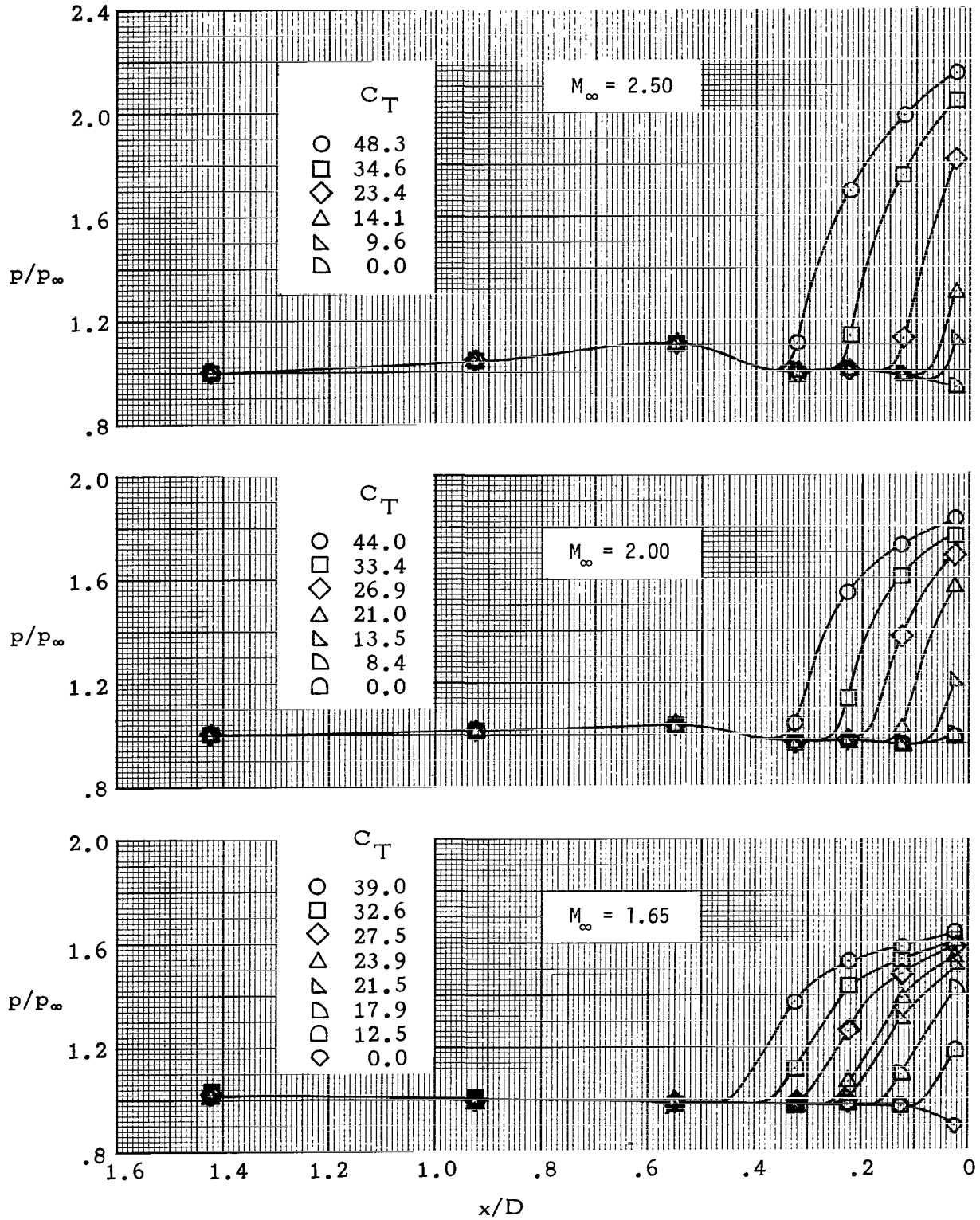


(a) $M_\ell$ = 1.7 nozzle.

Figure 8.- Afterbody pressure distributions for axisymmetric nozzles.

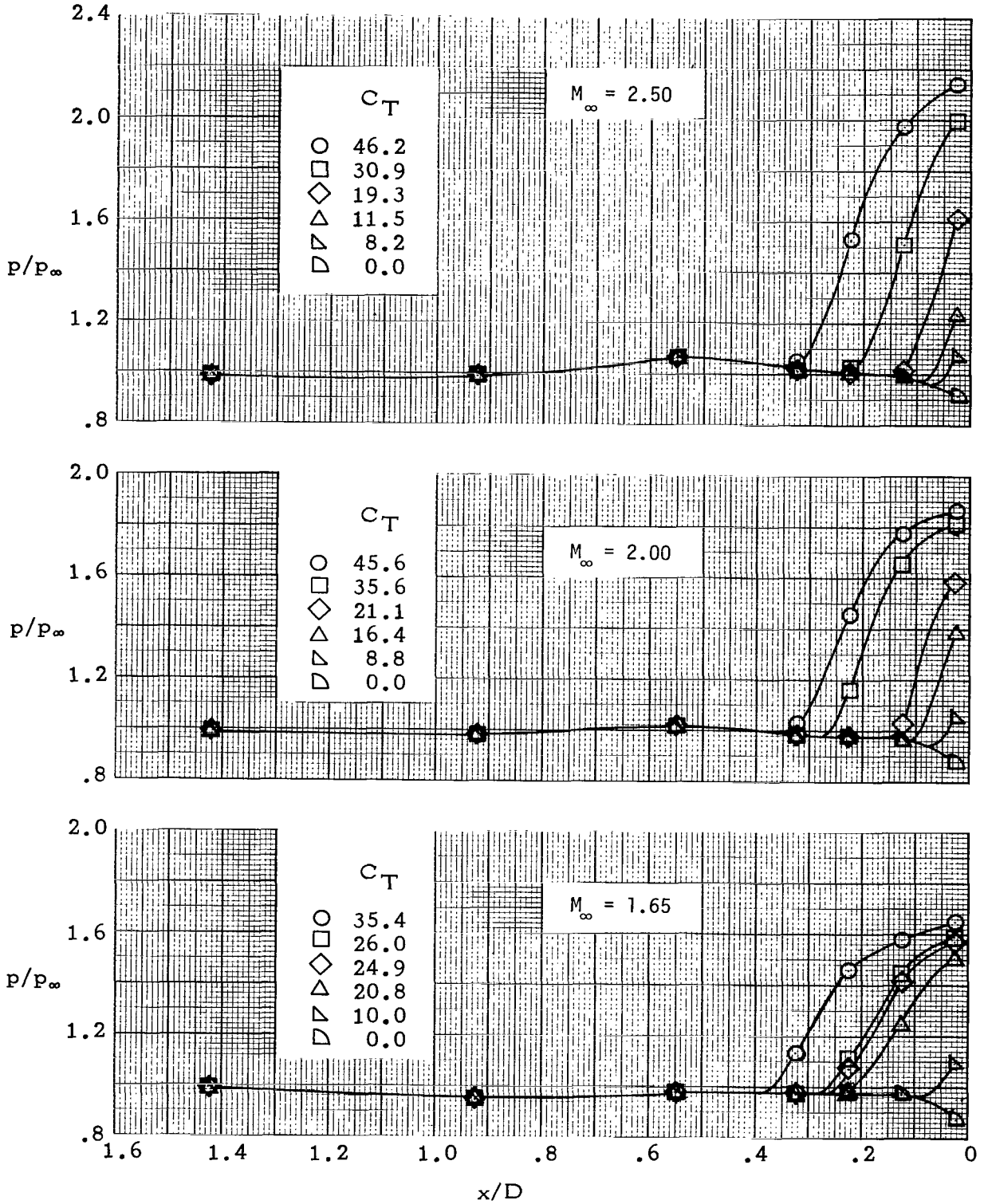


(b) $M_\ell$ = 2.0 nozzle.

Figure 8.- Continued.

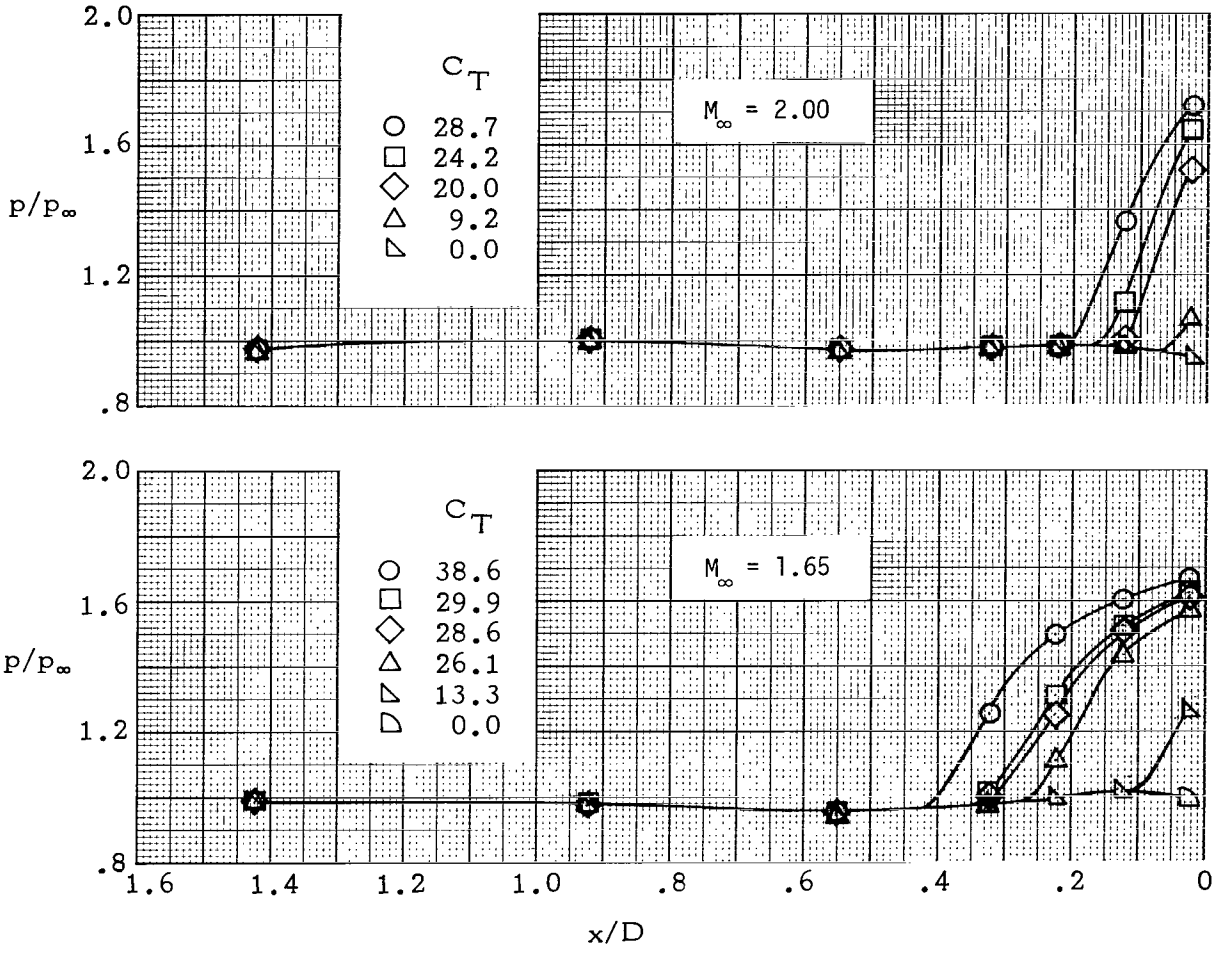


(c) $M_\ell$ = 2.4 nozzle.

Figure 8.- Continued.

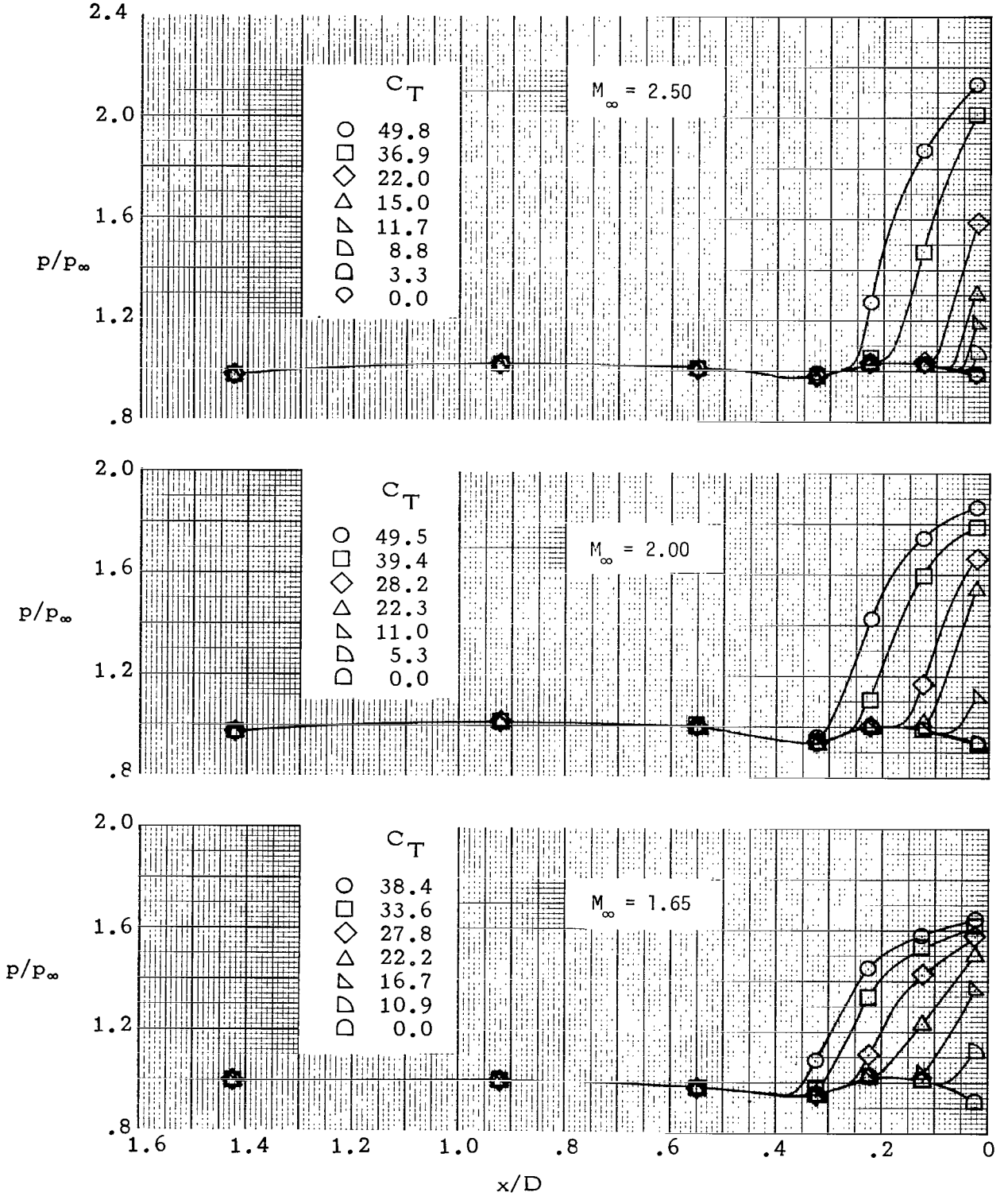


(d) $M_\ell$ = 2.7 nozzle.

Figure 8.- Concluded.

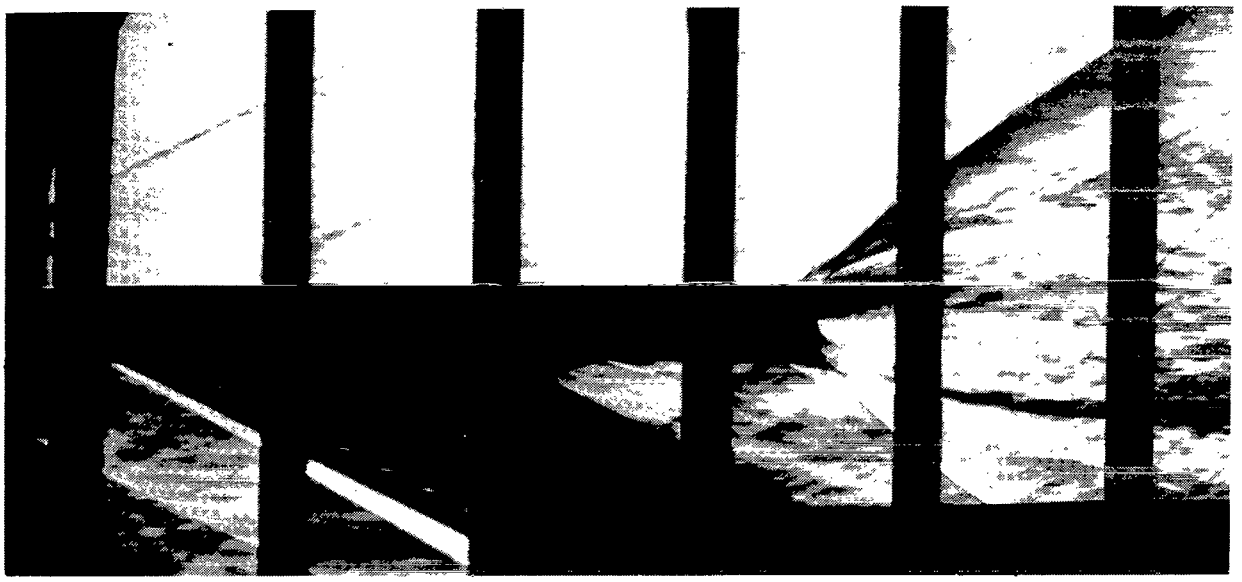

(a) $M_{\ell} = 2.7$ nozzle; $p_{t,j}/p_{\infty} = 455.7$; $C_T = 36.9$; $M_{\infty} = 2.50$.

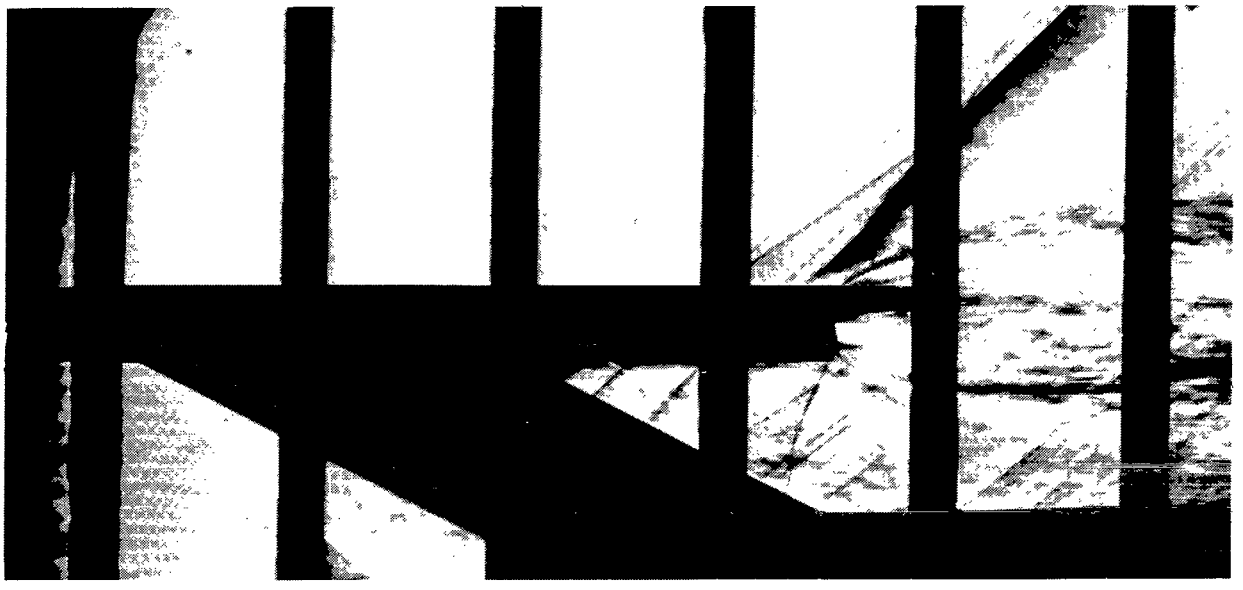

(b) $M_{\ell} = 2.0$ nozzle; $p_{t,j}/p_{\infty} = 123.4$; $C_T = 35.4$; $M_{\infty} = 1.65$.

L-82-123

Figure 9.- Selected schlieren photographs.

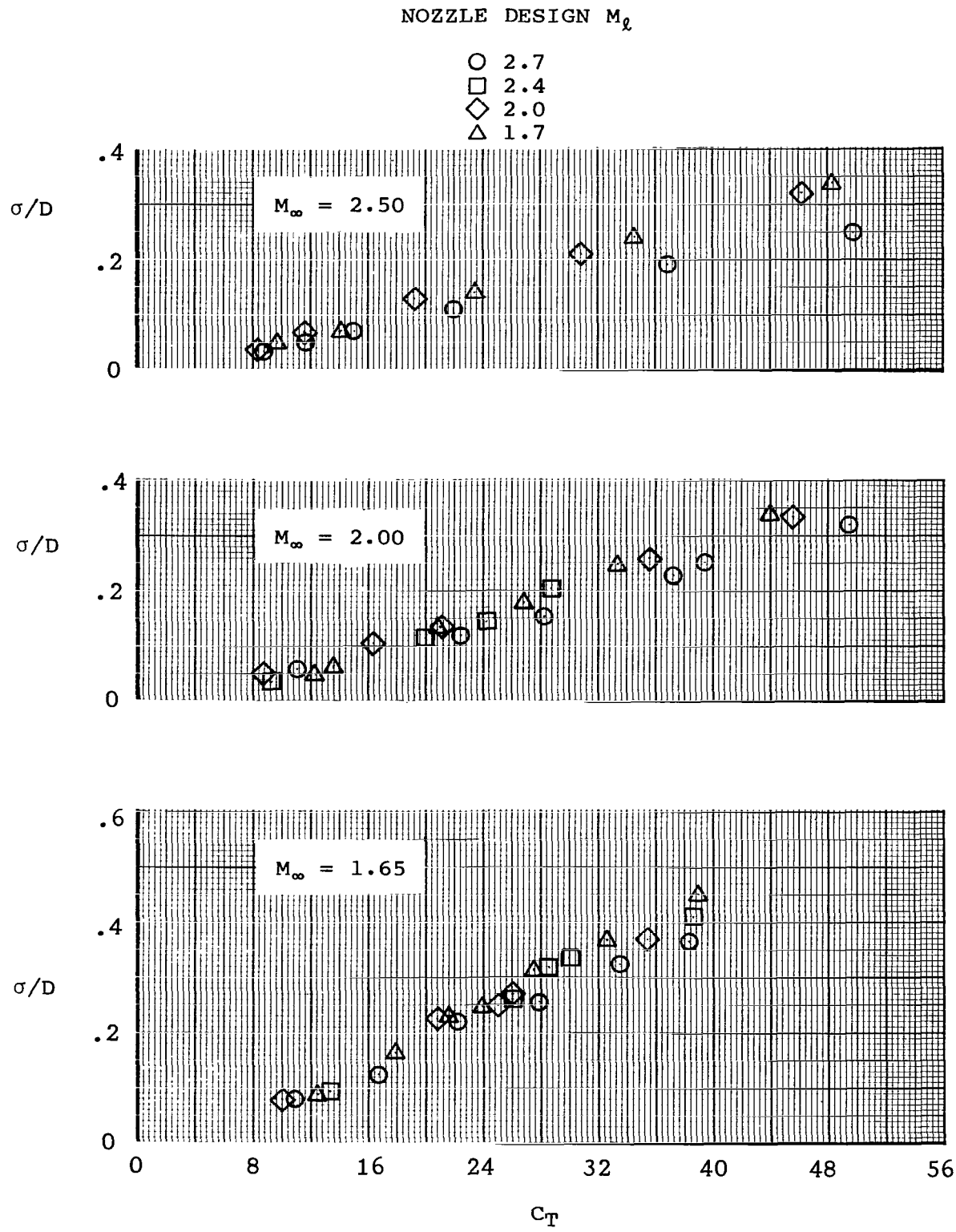


Figure 10.- Variation of disturbance distance with thrust coefficient for axisymmetric nozzles.

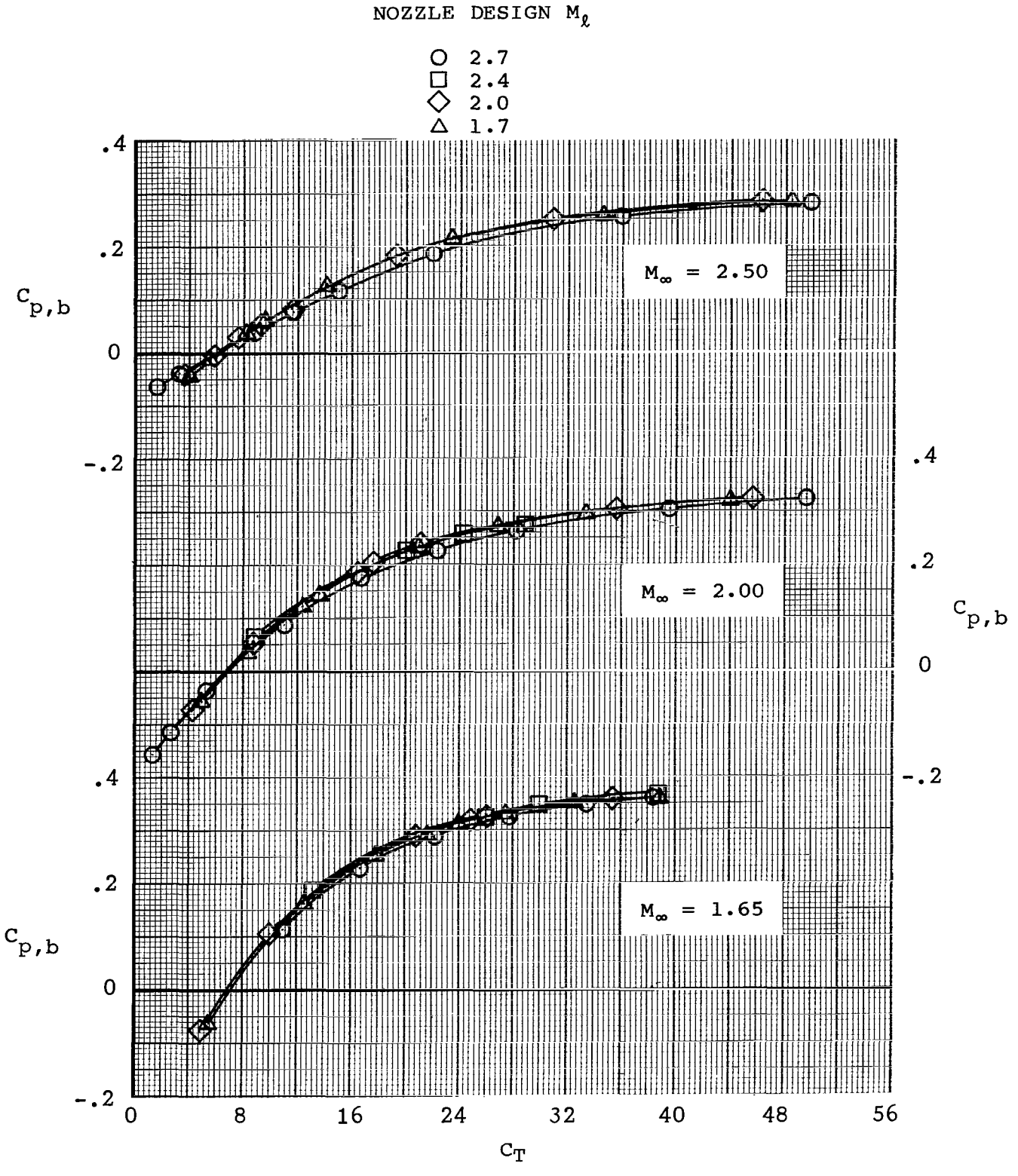


Figure 11.- Variation of base pressure coefficient with thrust coefficient for axisymmetric nozzles.

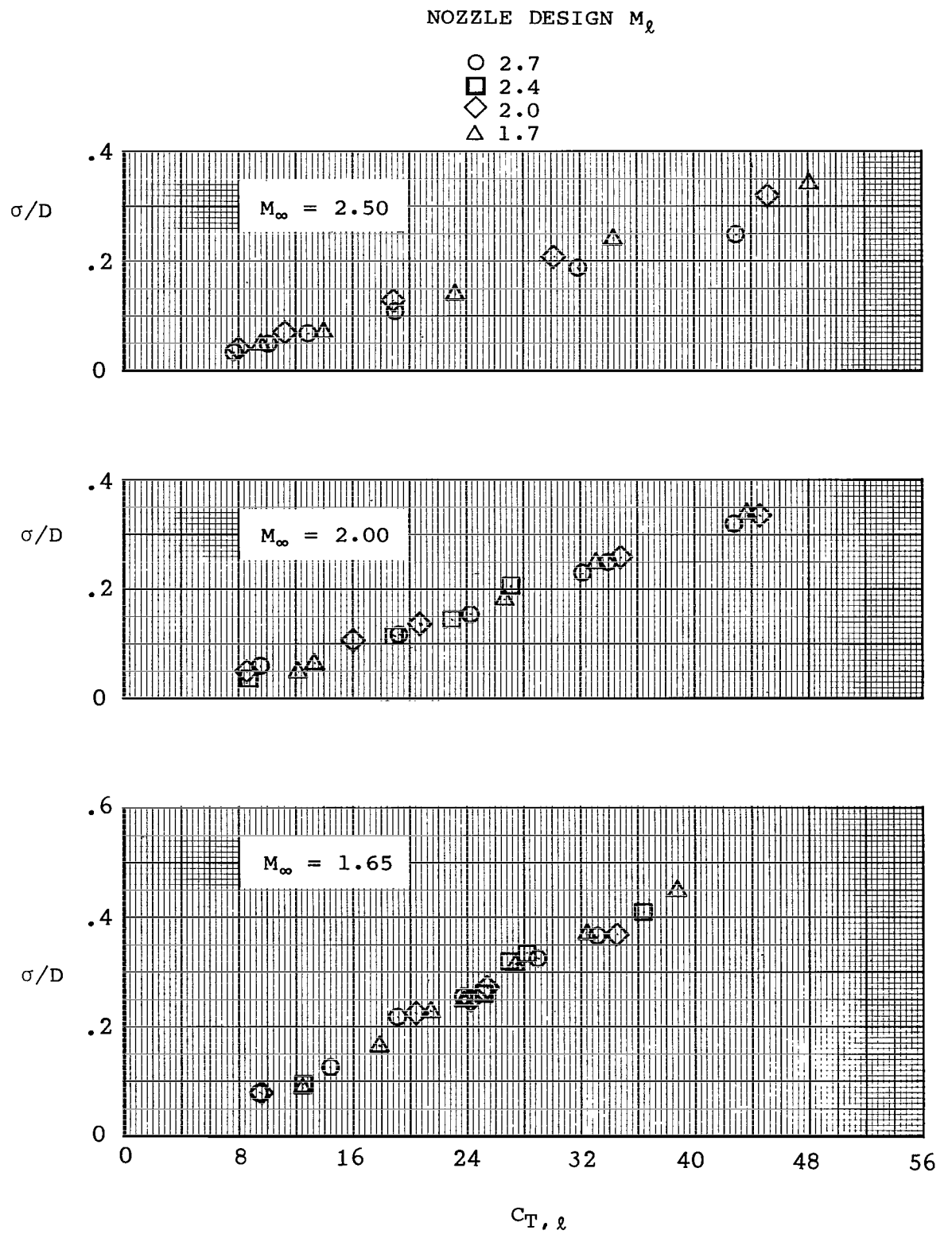


Figure 12.- Variation of disturbance distance with $C_{T,\ell}$ for axisymmetric nozzles.

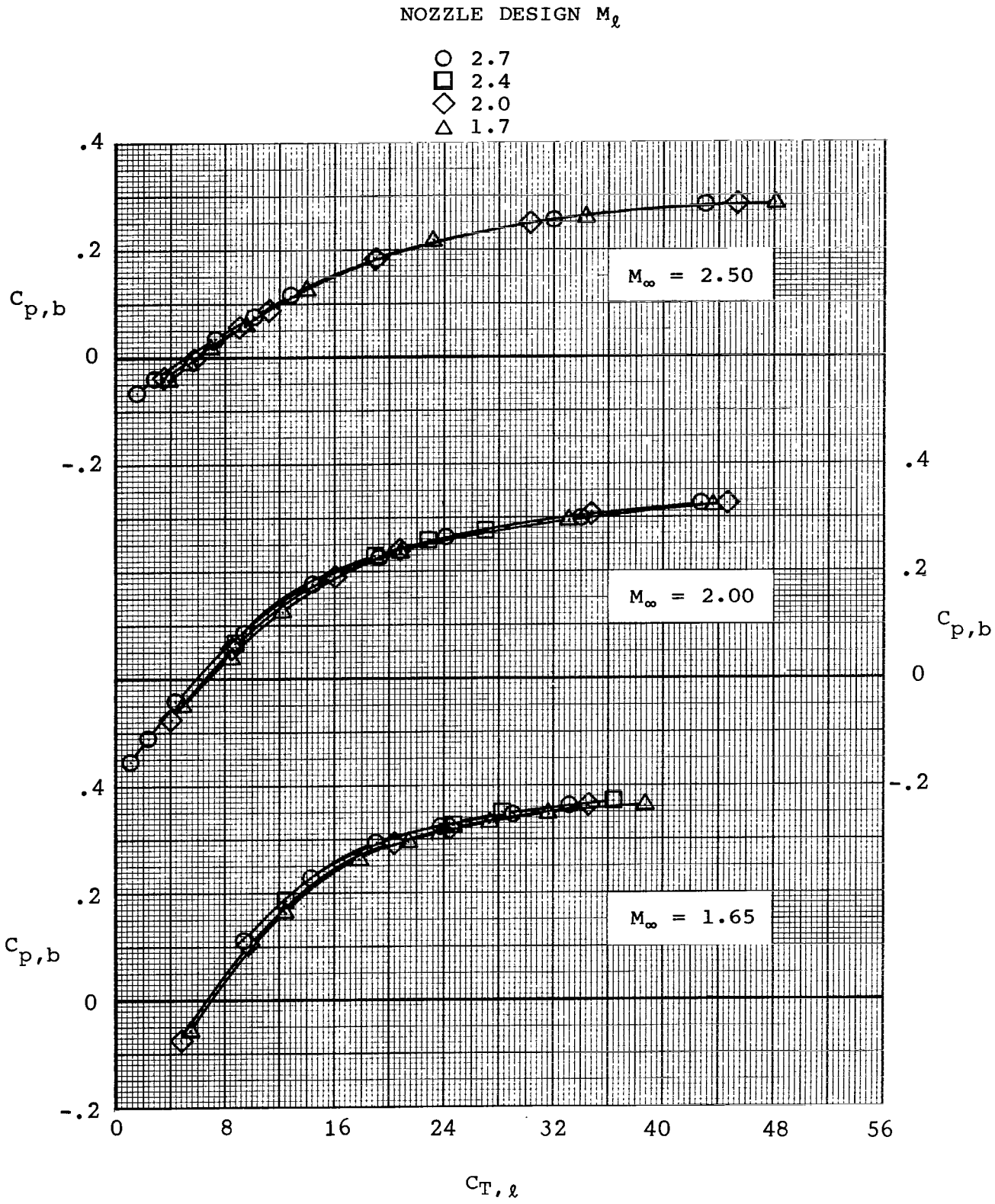


Figure 13.- Variation of base pressure coefficient with $C_{T,\ell}$ for axisymmetric nozzles.

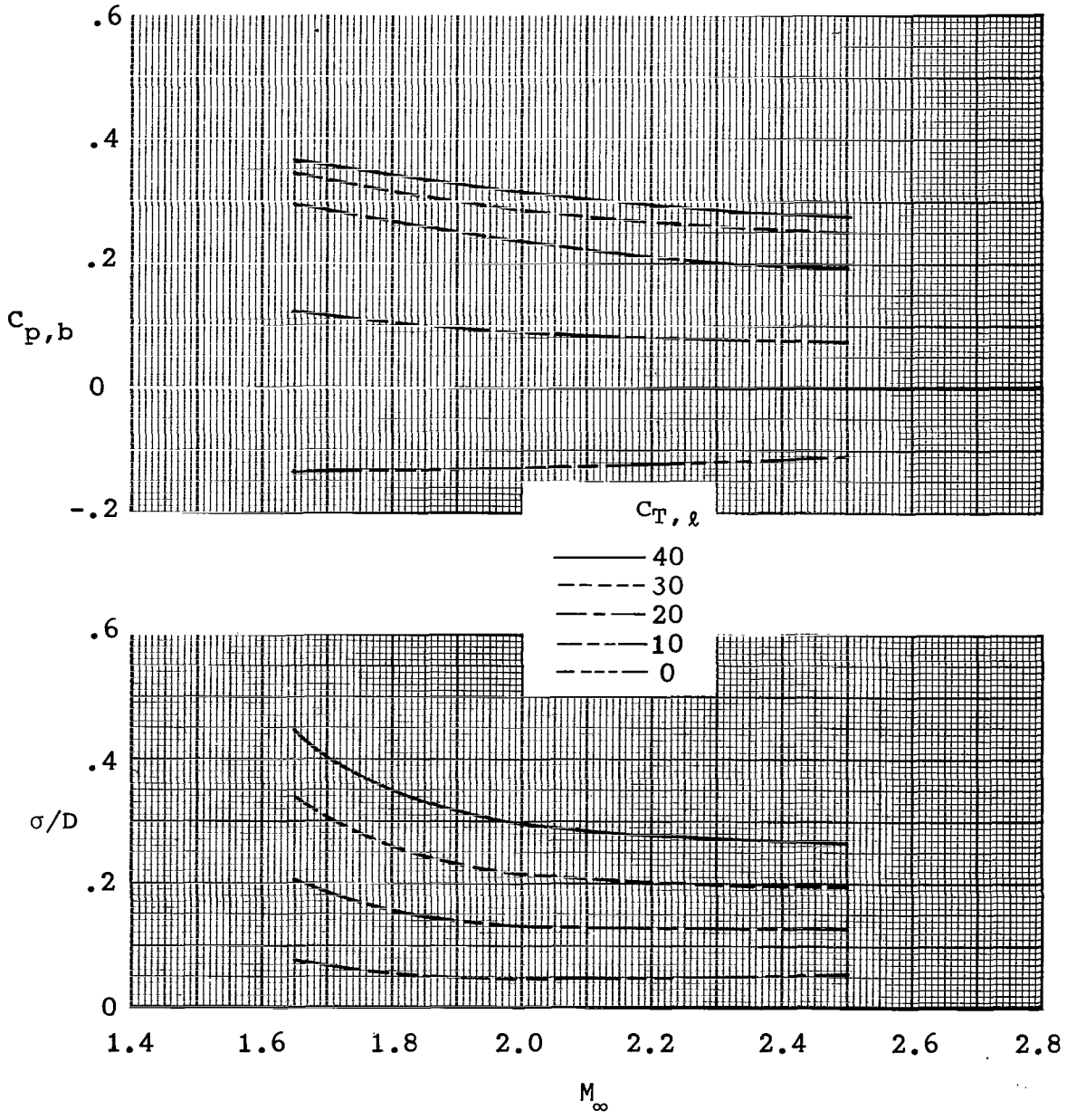


Figure 14.- Summary of plume-induced effects for four axisymmetric nozzles.

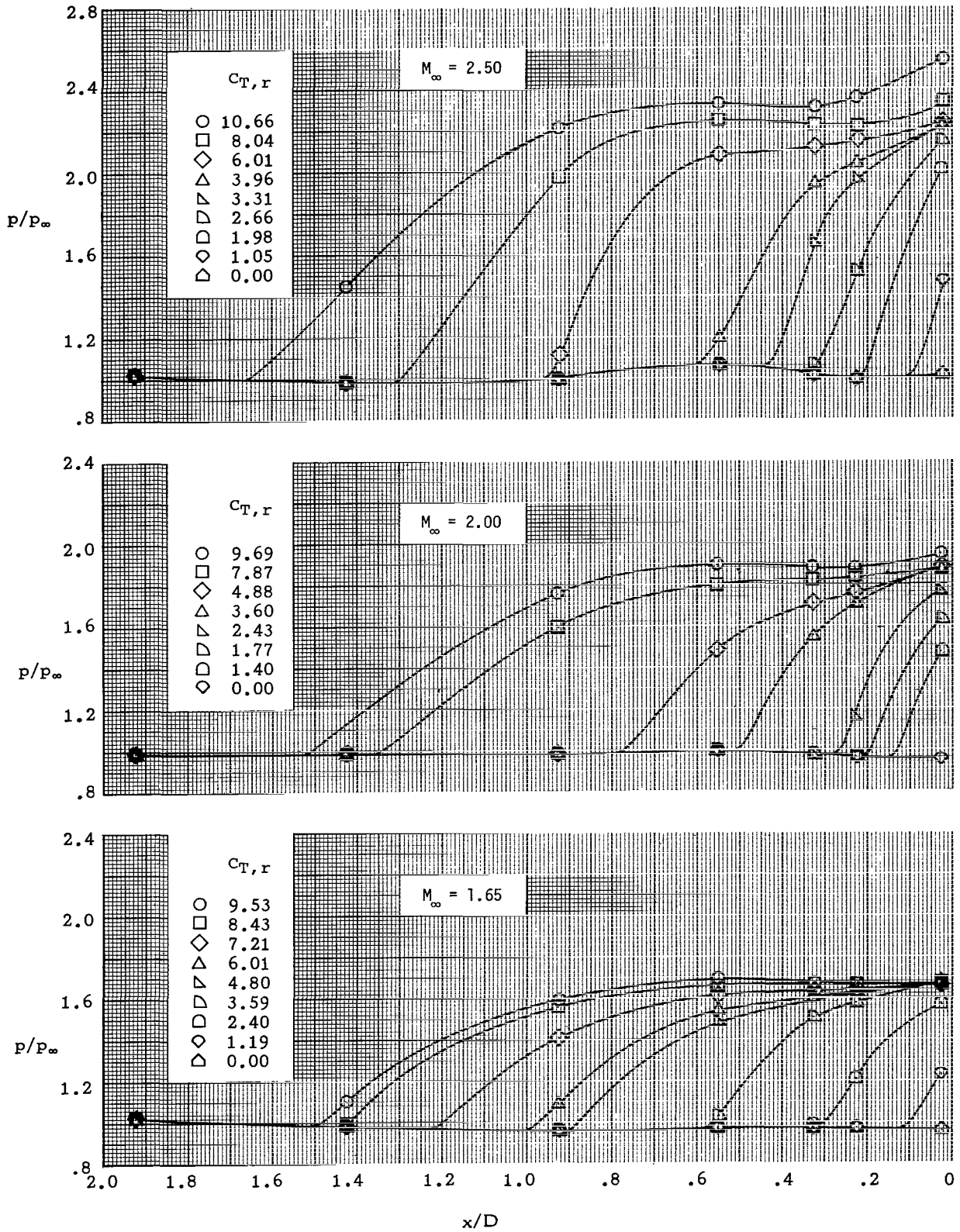


Figure 15.- Afterbody pressure distributions for normal air jet plume.

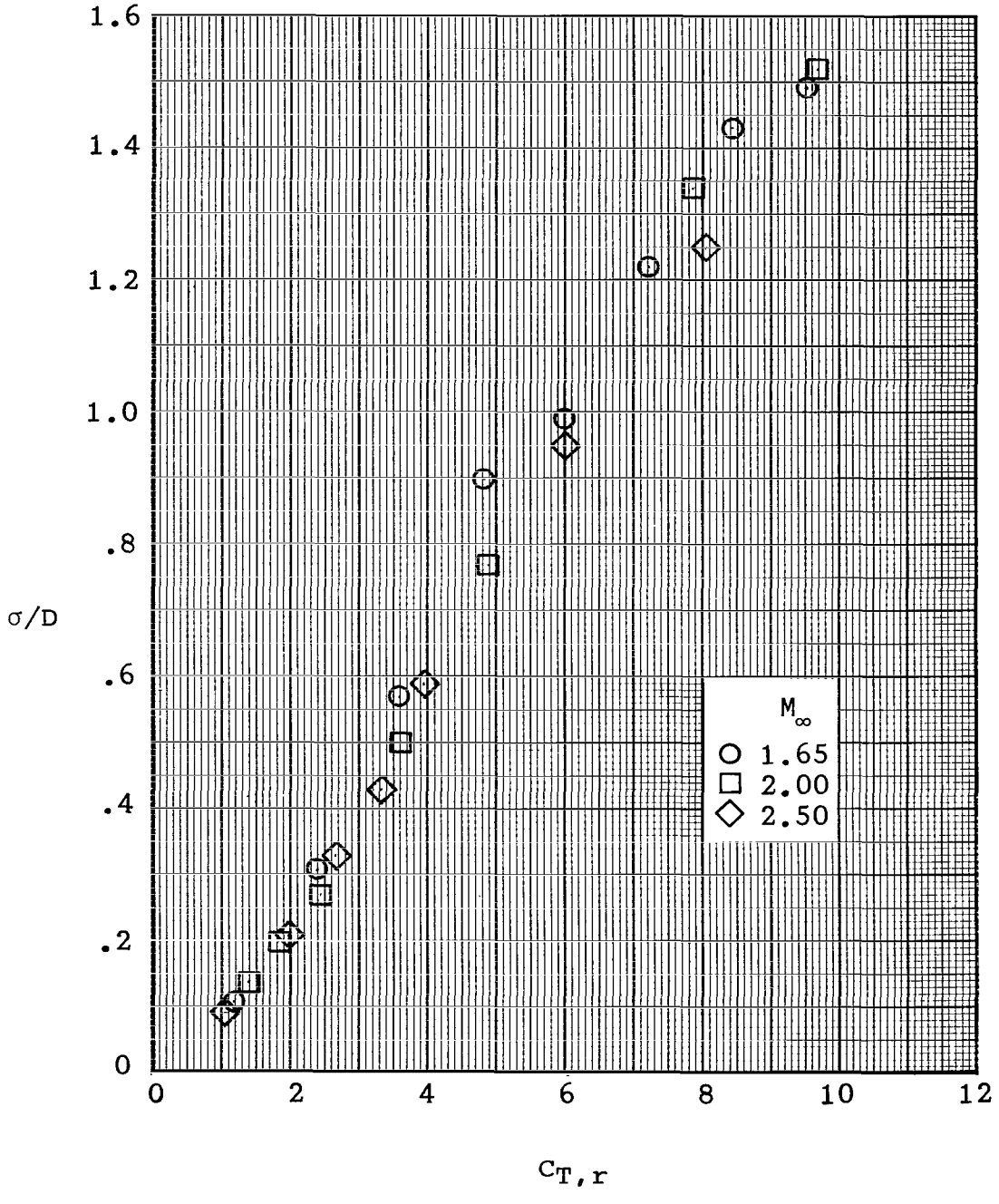


Figure 16.- Variation of disturbance distance with radial thrust coefficient for normal air jet plume.

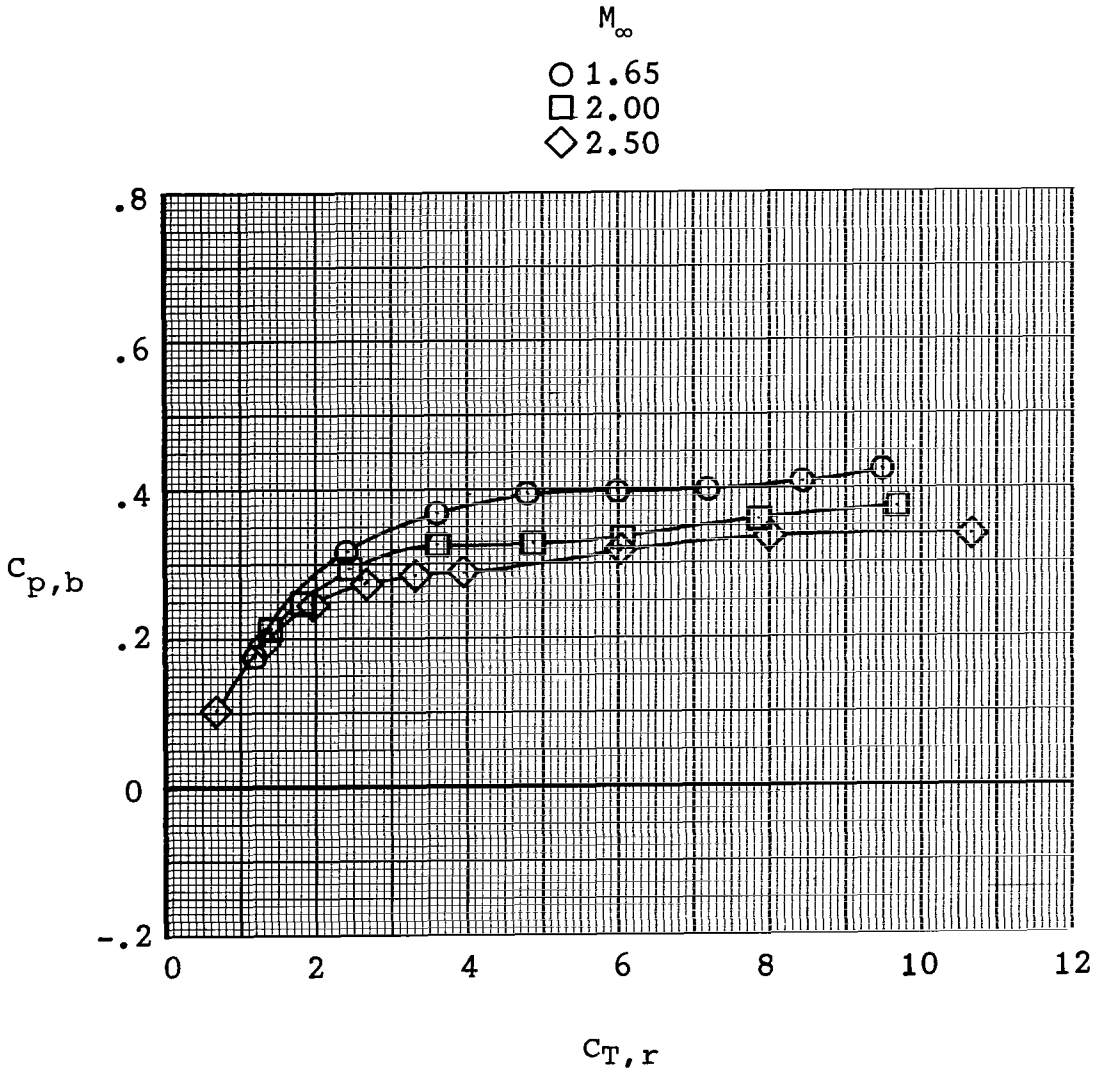


Figure 17.- Variation of base pressure coefficient with radial thrust coefficient for normal air jet plume.

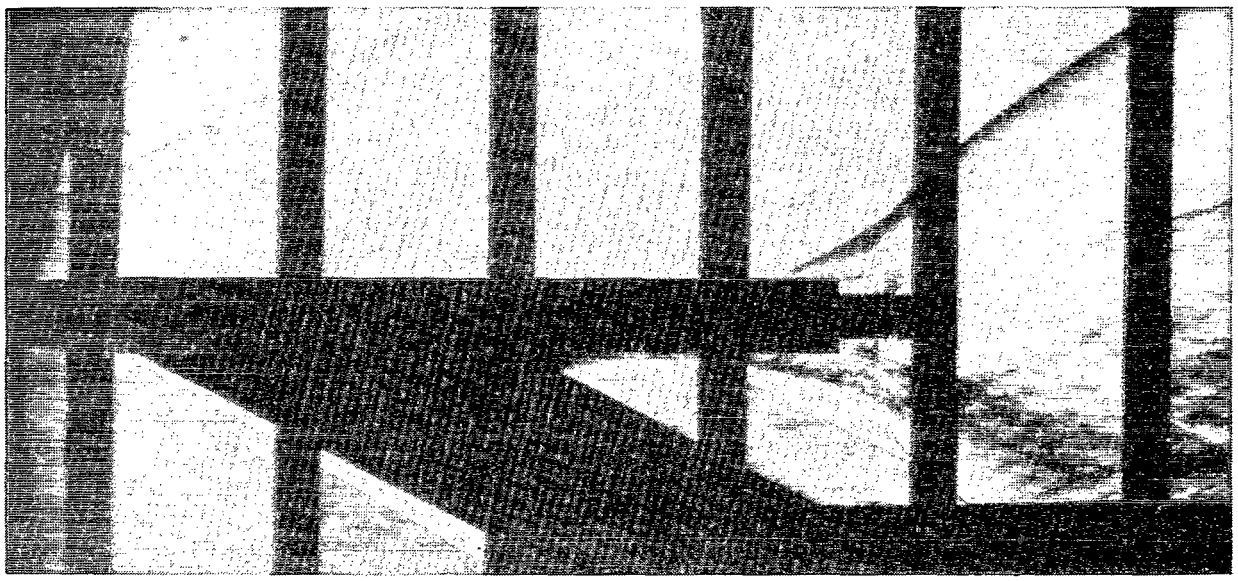

(a) $M_\infty = 2.50$; $C_{T,r} = 3.96$.

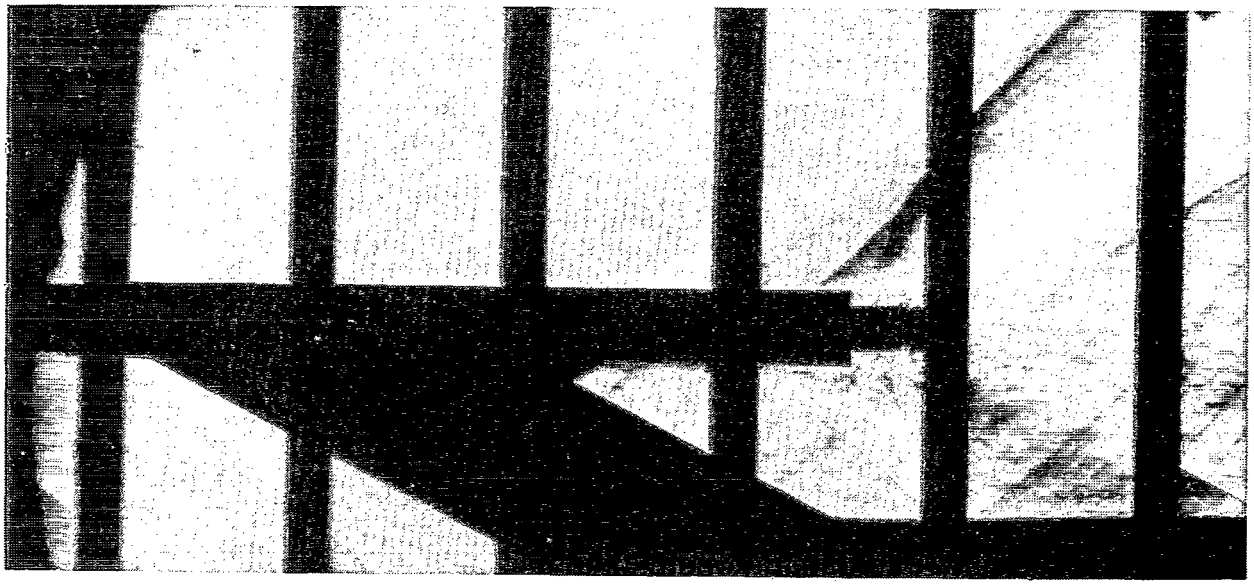

(b) $M_\infty = 1.65$; $C_{T,r} = 3.59$.

L-82-124

Figure 18.- Schlieren photographs for normal air jet plume.

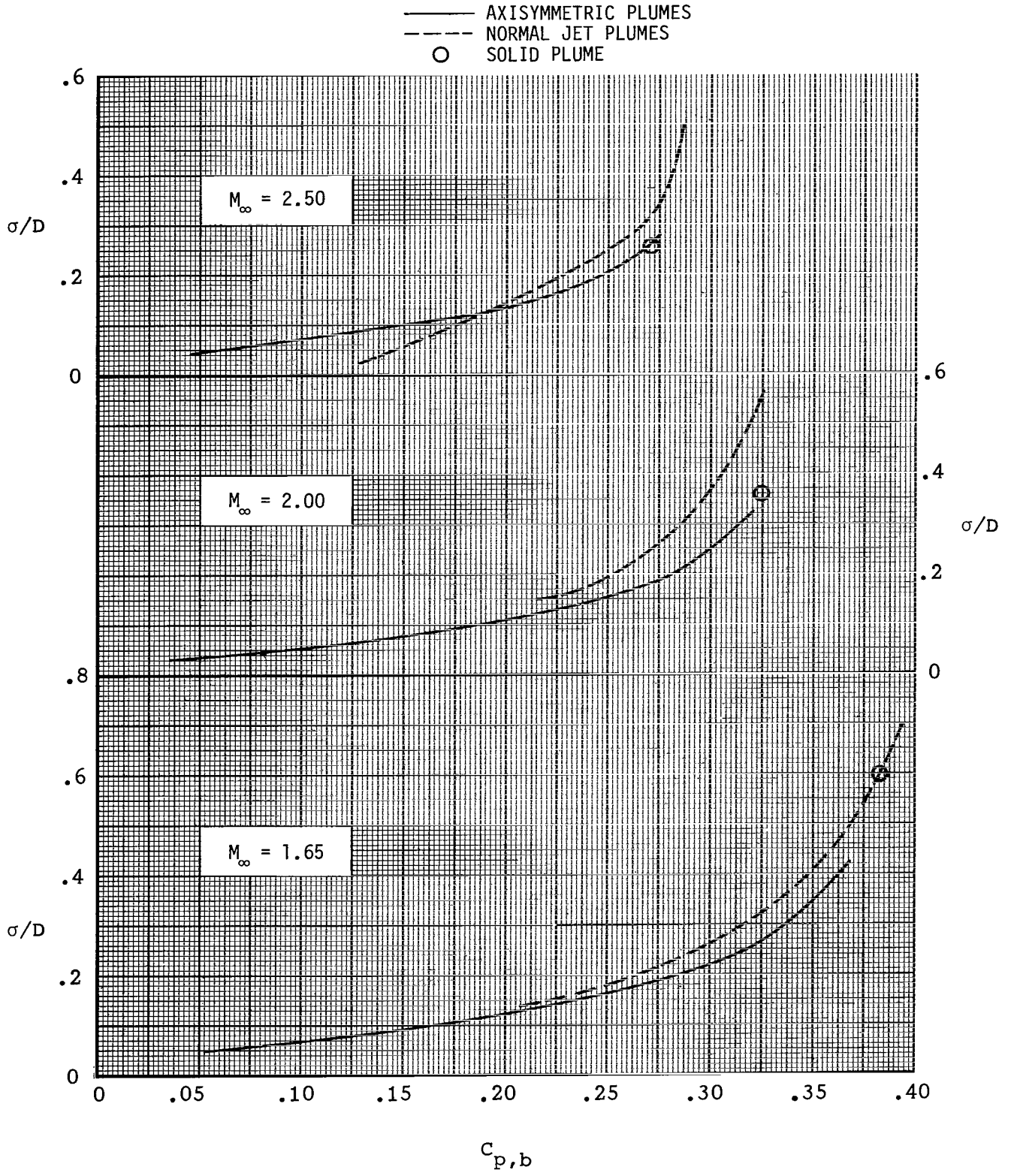


Figure 19.- Comparison of induced afterbody and base effects for axisymmetric, normal jet, and solid plumes.

| 1. Report No. | 2. Government Accession No. | 3. Recipient's Catalog No. |
|---|---|---|
| NASA TP-2005 | | |

| 4. Title and Subtitle | 5. Report Date |
|---|---|
| EFFECTS OF AXISYMMETRIC AND NORMAL AIR JET PLUMES AND SOLID PLUME ON CYLINDRICAL AFTERBODY PRESSURE DISTRIBUTIONS AT MACH NUMBERS FROM 1.65 TO 2.50 | April 1982 |
| | 6. Performing Organization Code: 505-43-23-02 |
| 7. Author(s): Peter F. Covell | 8. Performing Organization Report No.: L-14883 |
| | 10. Work Unit No. |
| 9. Performing Organization Name and Address: NASA Langley Research Center, Hampton, VA 23665 | 11. Contract or Grant No. |
| | 13. Type of Report and Period Covered: Technical Paper |
| 12. Sponsoring Agency Name and Address: National Aeronautics and Space Administration, Washington, DC 20546 | 14. Sponsoring Agency Code |

15. Supplementary Notes

16. Abstract

A wind-tunnel investigation of the interference effects of axisymmetric nozzle air plumes, a solid plume, and normal air jet plumes on the afterbody pressure distributions and base pressures of a cylindrical afterbody model has been conducted at Mach numbers from 1.65 to 2.50. The axisymmetric nozzles, which varied in exit lip Mach number from 1.7 to 2.7, and the normal air jet nozzle were tested at jet pressure ratios from 1 (jet off) to 615. The tests were conducted at an angle of attack of 0° and a Reynolds number per meter of $6.56 \times 10^6$. The results of the investigation show that the solid plume induces greater interference effects than those induced by the axisymmetric nozzle plumes at the selected underexpanded design conditions. A thrust coefficient parameter based on nozzle lip conditions was found to correlate the afterbody disturbance distance and the base pressure between the different axisymmetric nozzles. The normal air jet plume and the solid plume induce afterbody disturbance distances similar to those induced by the axisymmetric air plumes when base pressure is held constant.

| 17. Key Words (Suggested by Author(s)) | 18. Distribution Statement |
|---|---|
| Jet plume interference effects<br>Afterbody<br>Supersonic free-stream Mach numbers | Unclassified - Unlimited<br>Subject Category 02 |

| 19. Security Classif. (of this report) | 20. Security Classif. (of this page) | 21. No. of Pages | 22. Price |
|---|---|---|---|
| Unclassified | Unclassified | 33 | A03 |

For sale by the National Technical Information Service, Springfield, Virginia 22161

NASA-Langley, 1982

National Aeronautics and
Space Administration

Washington, D.C.
20546

Official Business
Penalty for Private Use, $300

THIRD-CLASS BULK RATE

Postage and Fees Paid
National Aeronautics and
Space Administration
NASA-451

U.S.MAIL

NASA

POSTMASTER: If Undeliverable (Section 158
Postal Manual) Do Not Return